Archives of Civil and Mechanical Engineering (2025) 25:23
https://doi.org/10.1007/s43452-024-01085-3

ORIGINAL ARTICLE

Estimating fundamental frequency of masonry arches under elevated temperature: numerical analysis and validation using ambient vibration tests

Ahmet Can Altunişik[1,2,3] · **Muhammed Mustafa Öztürk**[4] · **Ali Fuat Genç**[1] · **Ali Kaya**[5] · **Yunus Emrahan Akbulut**[1] · **Fezayil Sunca**[1] · **Murat Günaydin**[1]

Received: 24 April 2024 / Revised: 23 September 2024 / Accepted: 16 October 2024
© Wroclaw University of Science and Technology 2024

Abstract

In this study, the changing of dynamic characteristics of masonry arches at varying geometric parameters and temperature histories was investigated through a combination of experimental and numerical methods. First, the dynamic characteristics of laboratory-built arch models were determined both pre- and post-high-temperature test using ambient vibration testing. Then, the finite element (FE) models of the arches were developed for both, allowing for dynamic characteristics to be assessed numerically. To refine the accuracy of numerical models, FE analyses were adjusted based on experimental data. These updated FE models were used to investigate the dynamic characteristics of arches with different spans, heights, widths, and thicknesses under different temperature history scenarios. Finally, utilizing the data repository obtained, formulation and graphs/charts, providing valuable insights into the dynamic response of masonry arches under fire conditions, were developed and presented for practical application. The experimental study revealed that the natural frequencies of arches decreased by 55% with increasing temperature exposure.

Keywords Ambient vibration test · High temperature · Fire · Masonry arch · Dynamic characteristics · Finite element analyses

1 Introduction

Historic structures, pivotal in comprehending and contextualizing distinct epochs of civilization, serve as invaluable markers of cultural heritage and identity. Frequently employing masonry techniques inherited from antiquity, these architectural marvels stand as enduring symbols of human ingenuity. Hence, elucidating the structural behaviour of masonry structures holds paramount significance not only in the field of structural engineering, but also for nations characterized by the prevalence of such architectural forms.

✉ Ahmet Can Altunişik
ahmetcan8284@hotmail.com

Muhammed Mustafa Öztürk
mmustafa.ozturk@gop.edu.tr

Ali Fuat Genç
af.genc@ktu.edu.tr

Ali Kaya
akaya@artvin.edu.tr

Yunus Emrahan Akbulut
emrahan@ktu.edu.tr

Fezayil Sunca
fezayilsunca@ktu.edu.tr

Murat Günaydin
muratgunaydin@ktu.edu.tr

1 Department of Civil Engineering, Karadeniz Technical University, 61080 Trabzon, Turkey

2 Earthquake and Structural Health Monitoring Research Center, Karadeniz Technical University, Trabzon, Türkiye

3 Dynamic Academy Software, Construction Ind. Trade. Co., Ltd. Şti, 61080 Trabzon, Türkiye

4 Department of Civil Engineering, Tokat Gaziosmanpaşa University, Tokat, Türkiye

5 Department of Environmental Engineering, Artvin Çoruh University, Artvin, Türkiye

Published online: 10 November 2024

Finite element (FE) analysis is the numerical determination of the static and dynamic behaviour of structures [1]. FE model updating holds significant importance in the realm of historical structures, where accurate representation of structural behaviour is paramount. Due to the inherent complexities and uncertainties associated with historical masonry constructions, including variations in material properties, boundary conditions, degradation over time, and unknown construction methods, traditional FE models may lack precision in capturing the intricacies of their dynamic response. Consequently, the improving of FE models through updating procedures becomes imperative to enhance their predictive capabilities and account for these uncertainties. By integrating data obtained from non-destructive testing techniques, FE models can be calibrated to better reflect the actual behaviour of historic structures, mitigating the effects of uncertainties and improving the reliability of structural analyses. The final FE model provide a more accurate depiction, suggesting its potential applications in areas such as damage detection and structural health monitoring.

The ambient vibration testing (AVT) is a non-destructive procedure that enables the detailed extraction of dynamic characteristics, such as natural frequencies, mode shapes, and damping ratios. AVT is typically implemented by strategically placing accelerometers on the structure to capture ambient vibrations. These vibrations are then processed to extract the dynamic characteristics. Because the method obtains real-time data from the structure, it is widely used in damage detection, structural health monitoring and, in particular, FE model updating. In the literature, this method was used for different kinds of structures such as historical arch bridge [2], masonry monuments [3], bell tower [4], masonry mosque [5], and masonry minaret [6]. Monitoring changes in dynamic characteristics and structural behaviour over time offers a practical and dependable method. This approach proves especially useful in assessing structural impacts caused by various factors such as fire, damage, or restoration efforts [7].

Pillars, arches, vaults, and domes are the main load-bearing systems of the historic masonry structures. The masonry arch element holds significant importance in historical structures due to its unique structural properties and architectural versatility. By distributing weight evenly along its curved shape, arches efficiently bear loads and provide stability, allowing for the construction of expansive openings without the need for additional support columns. This architectural innovation not only enhances structural integrity, but also facilitates the creation of grand, open interior spaces, characteristic of many historical buildings. Also, the enduring durability of masonry arches contributes to the longevity of historical structures. For this reason, the arch elements play an important role in determining the behaviour of this type of structures.

Historic sites face substantial risks from fires, as evidenced by incidents such as the blaze at Windsor Castle in England in 1992, the fire that affected the Haydarpasa Station in Istanbul, Turkey, in 2010, and the damage to Ibrahim Tevfik Efendi Beach Palace in Istanbul, Turkey, in 2013. Additionally, the National Museum of Brazil in Rio de Janeiro experienced a devastating fire in 2018, while Notre Dame Cathedral in Paris, France, suffered a significant fire in 2019. Historical structures built before the advent of modern fire safety standards often do not comply with current fire safety regulations. As a result, they are susceptible to partial damage or potential collapse when exposed to fire. It should be noted that, in addition to fire-resistant design of historical structures, it is also important to restore the damaged historical structures due to the fire with as little intervention as possible [8]. Masonry arches play an important role in the load-bearing system of historic structures and generally remain standing after a fire. Efforts should prioritize the retention of the current structural elements to the greatest extent feasible, preserving their authenticity and integrity. The replacement decision can only be made if the change in structural behaviour is known. Here the question arises: to what extent does the structural behaviour/dynamic characteristics change in masonry structures, especially in arches which constitute a significant part of the load-bearing system, when exposed to fire? And how can we catch the structural change? This study seeks to provide answers to these questions. To achieve this, the prescribed procedure, demonstrated in Fig. 1, includes the following steps:

- ✓ Identifying the material properties of masonry units and walls,
- ✓ Construction of masonry arch models,
- ✓ Ambient vibration testing to identify the dynamic characteristics of the arch models,
- ✓ High-temperature test and subsequent ambient vibration testing of the arch models to identify the dynamic characteristics of the arch models,
- ✓ Developing an initial FE model for the arch models,
- ✓ Updating the initial FE model to obtain the final FE models,
- ✓ Developing the formulation and creating the graphs/charts to evaluate the change of the dynamic characteristics with the multiple FE analysis of different parameters such as arch span, height, width, and thickness.

2 Masonry arch models and material properties

Two masonry arch models were constructed at the laboratory using hydraulic lime mortar andesite stone units. The arches are fixed to a rigid concrete raft foundation with dimensions

Fig. 1 Flowchart of the study

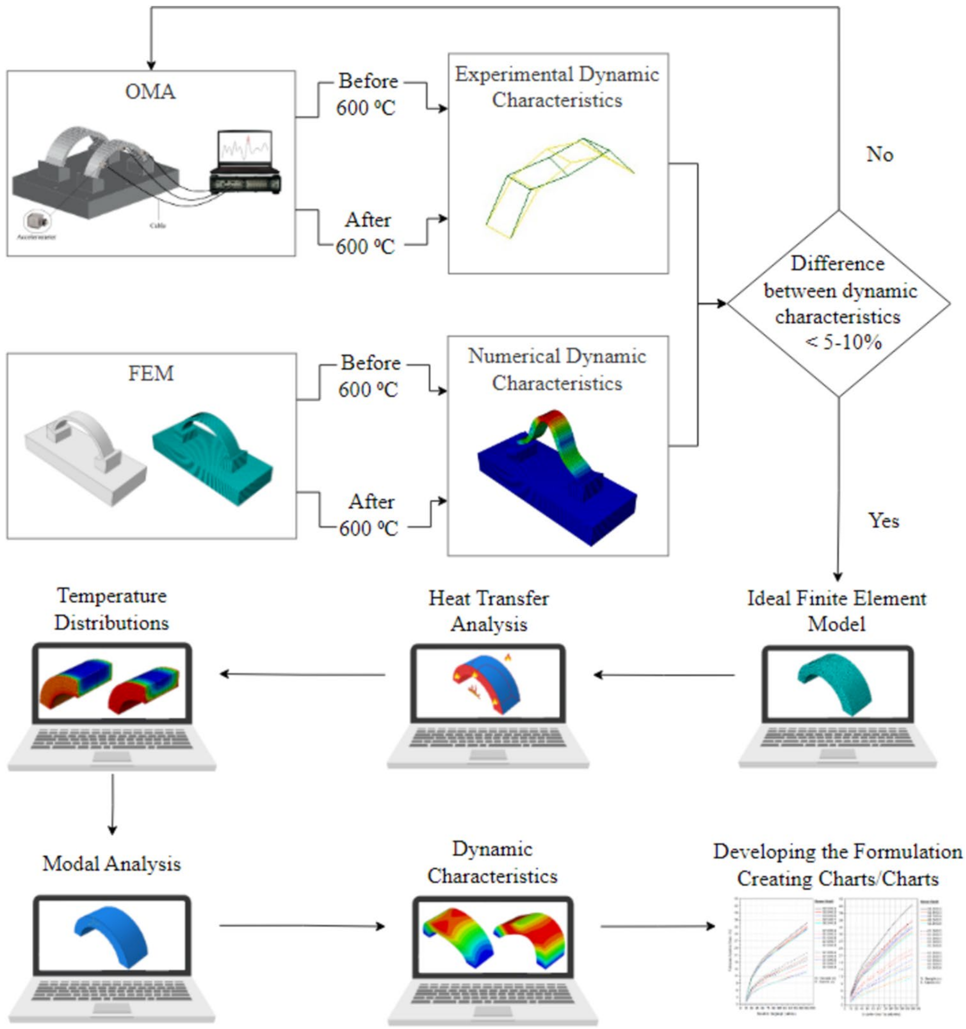

of 180 × 145 × 25 cm (length x width x height). Also, the reinforced arch piers were built to transfer the arch load to the foundation. The dimensions and construction stages of the arch models are given in Fig. 2 and Fig. 3, respectively.

The material properties of the masonry units and concrete were detailed for pre- and post-high-temperature effects. The compression and density tests were carried out using wall samples. The tests were repeated for exposure to high temperature (600 °C) and the results were compared with those obtained under room temperature conditions. The C45/55 class ready mixed concrete was used in the construction of the foundations. Six cube (15 × 15 × 15 cm) and four cylindrical concrete samples were taken to identify the compressive and splitting tensile strength and density of the concrete. The specimens were kept in a curing pool at 21 ± 2 °C for 28 days. Tables 1 and 2 show the test results. As can be seen from the table, the target strength value was achieved.

The wall samples were fabricated to obtain the average compressive strength and density of masonry wall units. As suggested by the ASTM C 1314-02a standard [9], the walls were built with three rows of 5 × 5 × 10 cm bricks. Also, five rows of 5 × 5 × 5 cm and 5 × 5 × 10 cm were built as suggested by TS EN 1052–1 standard [10]. Figure 4 shows the wall samples built.

The wall samples were covered with a polyethylene sheet for 3 days to allow them to cure, and at the end of this period the samples were left unprotected in the laboratory for 25 days. Some of the wall samples were then exposed to temperatures of 200 °C, 400 °C, 600 °C, and 800 °C in an electric furnace, using the temperature–time curve shown in Fig. 5. The samples that were removed from the temperature furnace were left to cool down in the laboratory environment (Fig. 6b).

For the wall samples stored in the laboratory environment, the average density value was determined. Then, the wall samples were exposed to the compressive strength test in accordance with the TS EN 1052–1 and ASTM C 1314-02a standards, as shown in Fig. 7. Tables 3 and 4 present the average comprehensive strength values and average density values of the wall samples, respectively. As can be seen, the

Fig. 2 Geometrical properties of the arch models

Dimension (cm)	Model-1	Model-2
Span (S)	100	100
Height (H)	50	50
Width (W)	20	30
Thickness (T)	5	5

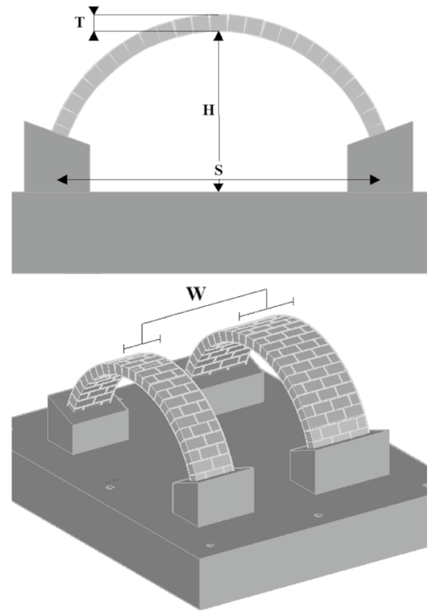

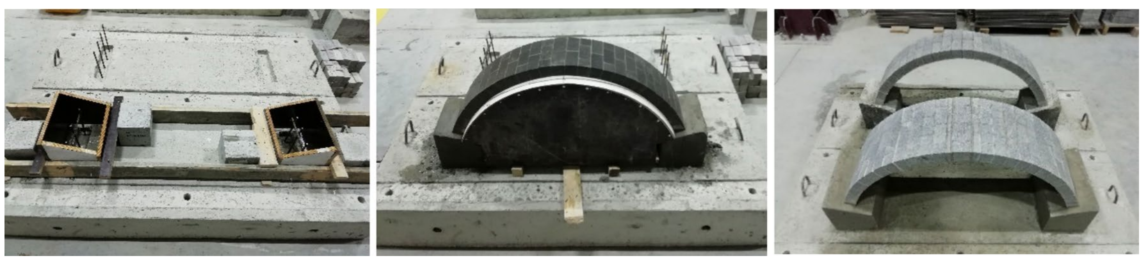

Fig. 3 Construction stages of the arch models

Table 1 Cubic sample results

Sample	Compressive strength (MPa)	Fracture load (kN)	Density (kg/m^3)
1	58.22	1310	2434
2	53.74	1209	2402
3	52.12	1172	2448
4	59.26	1333	2369
5	51.40	1156	2406
6	57.78	1300	2388

Table 2 Cylindrical sample results

Sample	Fracture load (kN)	Splitting tensile strength (MPa)
1	101	3.21
2	132	4.20
3	133	4.23
4	103	3.28

compressive strength and density values decrease significantly with increasing the temperature.

3 Dynamic characteristics for pre- and post-high-temperature exposure

Ambient vibration testing (AVT) is practised to obtain the dynamic characteristics of the models. Figure 8 presents a flowchart outlining the process for obtaining the dynamic characteristics of structures using AVT.

The AVT test equipment are: a B&K 3560 data acquisition system with 17 channels, B&K 4506 triaxial and B&K 4507 uniaxial accelerometers, and PULSE [11] and OMA [12] software. The frequency span selected was 0–300 Hz. Vibration signals were obtained by gathering data from nine accelerometers, which operated at intervals of 10 min. One accelerometer was (B&K 4507) used as a reference. For the data-gathering process, three accelerometers were moved from the external corners of the models to the opposite corners, as shown in Fig. 9. Figure 10 shows the measurement of the models.

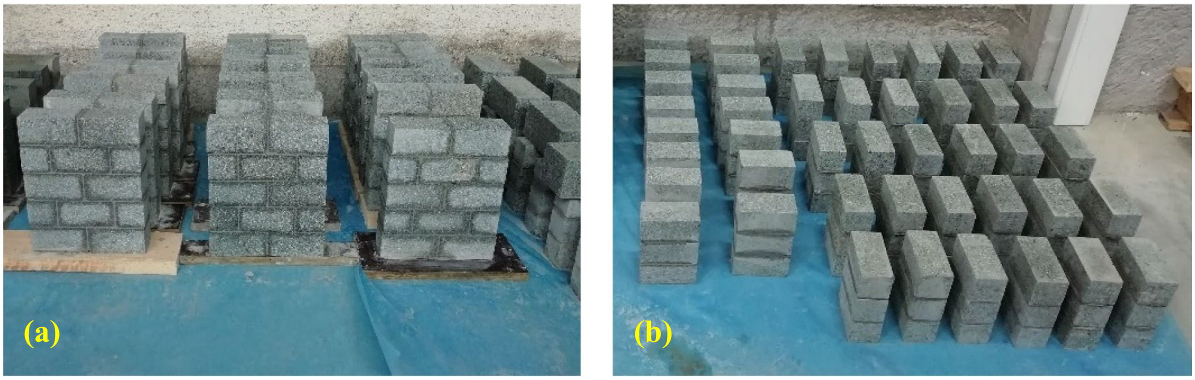

Fig. 4 Wall samples built according to: **a** TS EN 1052–1 and **b** ASTM C 1314-02a standards

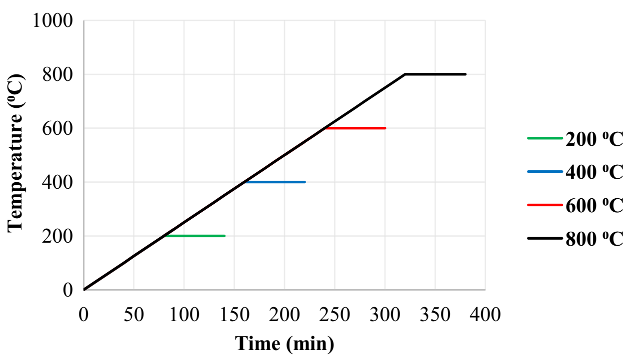

Fig. 5 The temperature–time curve utilized in the high-temperature tests of the samples

The test procedure was practised to obtain the change in dynamic characteristics after exposing the model to high temperatures. The peak temperature in the high-temperature test was selected as 600 °C. This is because higher temperatures could potentially cause severe damage to the structure. The rate of temperature increase was selected as 2.5 °C/min in accordance with the literature. Therefore, a test duration of 4 h was required to reach 600 °C. Following a 4-h duration of thermal exposure, the oven door was cautiously and gradually opened, allowing for the determination of the outer surface temperatures of the models subsequent to the test utilizing a pyrometer. Figure 11 shows the models both pre- and post-high-temperature test. Figure 12 shows the measurement of the model for the post-high-temperature test.

The enhanced frequency domain decomposition (EFDD) method was used to obtain the mode shapes and natural frequencies. The singular values of spectral density matrices (SVSDM) of the data set obtained by the EFDD method are given in Fig. 13.

The mode shapes obtained were the same for the pre- and post-high-temperature test. The first three experimental mode shapes were longitudinal mode, transverse mode, and vertical mode (Fig. 14).

Table 5 presents the comparison of natural frequencies for pre- and post-high-temperature test. As can be seen, a sharp decrease in natural frequencies occurred after high-temperature test. The maximum difference was 55% in the first mode for the first model and 48% in the second mode for the second model.

Fig. 6 Wall samples (**a**) exposed to fire and (**b**) cooling at the laboratory

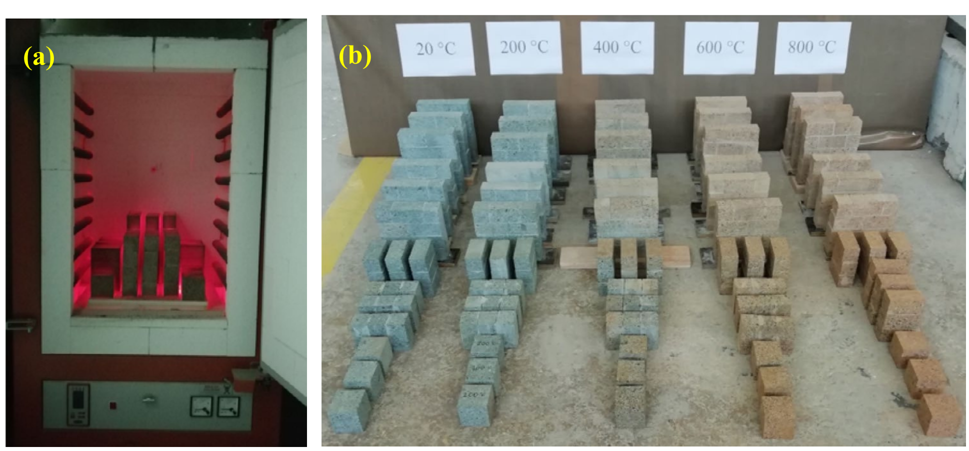

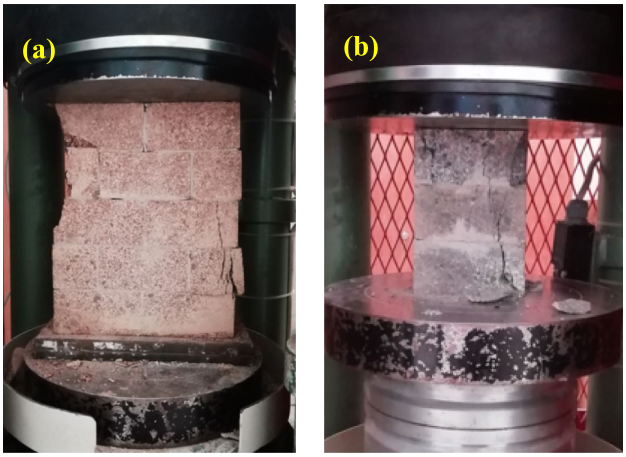

Fig. 7 Test procedure of wall samples: **a** TS EN 1052–1 and **b** ASTM C 1314-02a standards

Table 3 The tests results obtained from walls samples considering the TS EN 1052-1 for the different temperature values

Temperature (°C)	Area (cm²)	Volume (cm³)	Density (kg/m³)	Fracture load (kN)	Compressive strength (MPa)
20	100	2500	2300	285.1	28.51
200	100	2500	2235	281.2	28.12
400	100	2500	2124	208.3	20.83
600	100	2500	2099	103.7	10.37
800	100	2500	2038	80.2	8.02

Table 4 The tests results obtained from walls samples considering the ASTM C 1314-02a for the different temperature values

Temperature (°C)	Area (cm²)	Volume (cm³)	Density (kg/m³)	Fracture load (kN)	Compressive strength (MPa)
20	50	750	2305	160.70	32.14
200	50	750	2246	165.30	33.06
400	50	750	2119	94.20	18.84
600	50	750	2075	59.85	11.97
800	50	750	2031	35.30	7.06

4 Numerical studies

This part presents the FE analysis of models for pre- and post-high-temperature test. First, the initial FE model was developed for the case where there is no exposure to elevated temperature. Then the FE models were updated in accordance with experimental natural frequencies obtained from AVT to obtain the final FE models. Finally, the FE model of the post-high-temperature test was developed, and multiple thermal analyses were carried out taken into account different parameters of arch models such as height, span, width, and thickness to obtain the changing of dynamic characteristics with elevated temperatures. Based on the results, a repository was created to illustrate the formulations and graphs, aiming to practically determine the changes in stiffness due to the elevated temperature effect.

4.1 Initial FE models

The FE models of the laboratory models were developed in ABAQUS [13] software using C3D8R element type. The elasticity modulus of concrete raft foundation and arch piers was calculated as 35,801 MPa considering the target compressive strength proposed by TS500 [14]. Masonry arches were modelled with macro modelling approach. Various studies and design standards have different empirical formulae for the calculation of the elasticity modulus of masonry materials [15]. FEMA356 [16], Masonry Standards Joint Committee [17], TEC2018 [18], CSA S304 [19] and Eurocode 6 [20] multiply the masonry compressive strength by 550, 700, 750, 850, and 1000, respectively, to calculate the elasticity modulus. Also, researchers have proposed coefficients of 300 [21] and 500–600 [22]. Considering these coefficients, the elasticity modulus of masonry ranges from 1800 to 6100 MPa. A value of 3000 MPa was taken into account in the initial FE model. The Poisson ratio was taken as 0.2 for the masonry and concrete elements. Also, the density was considered as 2300 kg/m³ and 2400 kg/m³ for the masonry and concrete elements, respectively. As a boundary condition, the base was assumed to be fixed. Also, the mesh size was selected as 15 × 15 × 15 mm rectangular prism shaped. 104876 and 120882 solid elements were obtained for both models (Fig. 15). Figure 15 presents the FE models of both laboratory models.

Numerical natural frequencies obtained from the initial FE models were 72.32 Hz, 93.37 Hz and 142 Hz for Model 1, and 72.50 Hz, 116.6 Hz and 142.2 Hz for Model 2. Mode shapes of the models were obtained as longitudinal, transverse and vertical, respectively (Fig. 16). Table 6 presents a comparison of the experimental and numerical dynamic characteristics. This indicates that there is not good correlation between the experimental and numerical natural frequencies. The maximum difference was calculated as 19.62% for the first mode. The modal assurance criterion (MAC) is computed as a scalar constant that indicates the level of consistency between a modal vector and a reference modal vector. The MAC value ranges between 0.0 and 1.0, where 0 indicates no correlation and 1 represents complete correlation. The

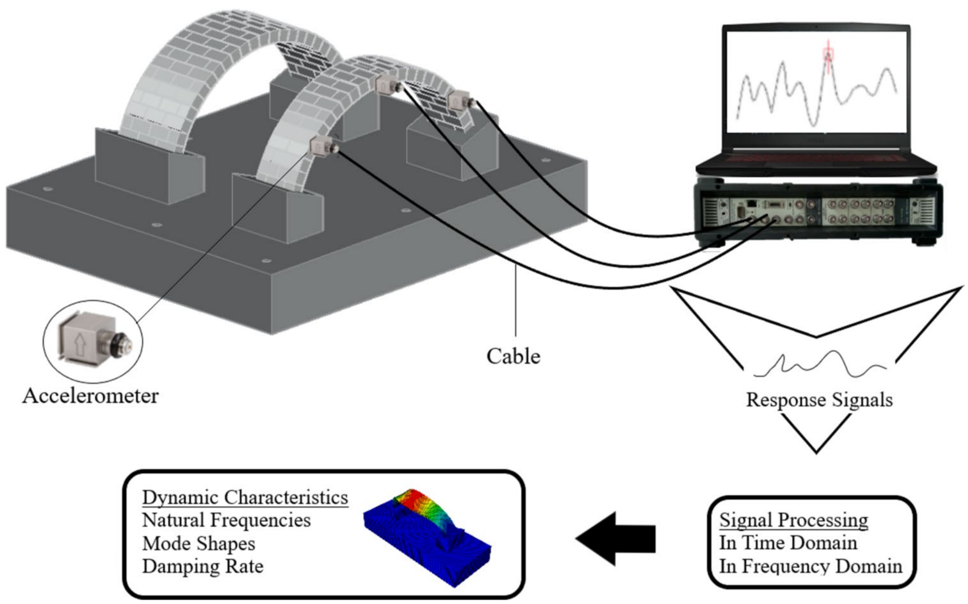

Fig. 8 Flowchart for the AVT of the models

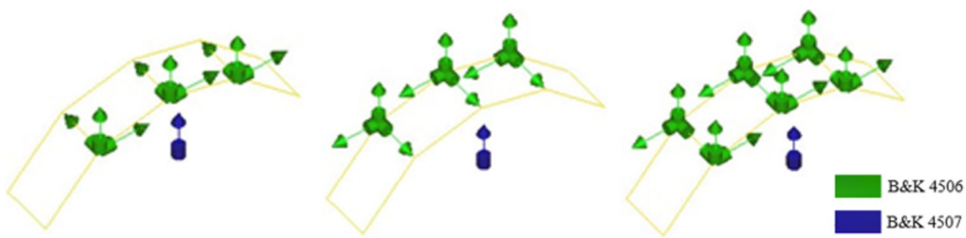

Fig. 9 View of modelling in Pulse software

Fig. 10 View of the AVT for the models

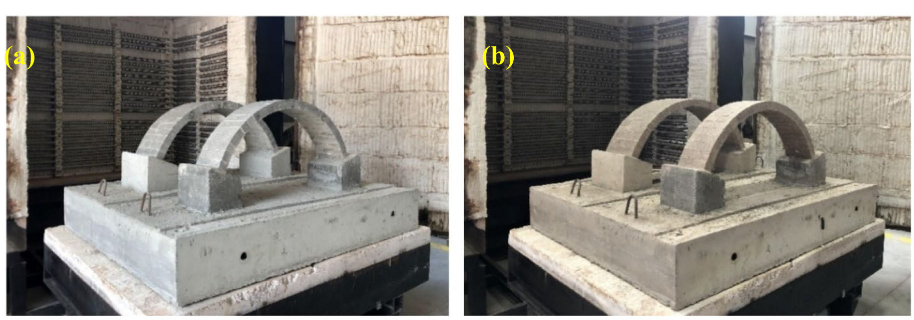

Fig. 11 View of models: **a** pre- and **b** post-high-temperature test

Fig. 12 View of the AVT of the model for the post-high-temperature test

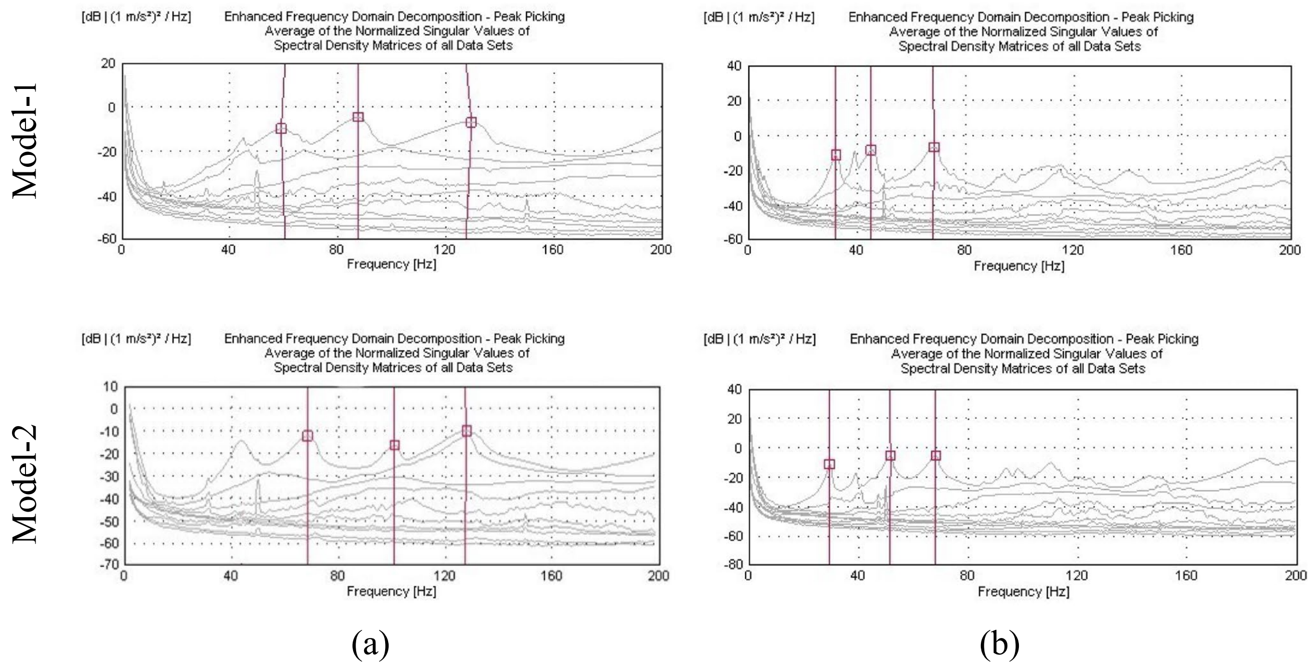

Fig. 13 SVSDM of the data sets obtained from the EFDD for the pre- and post-high-temperature test

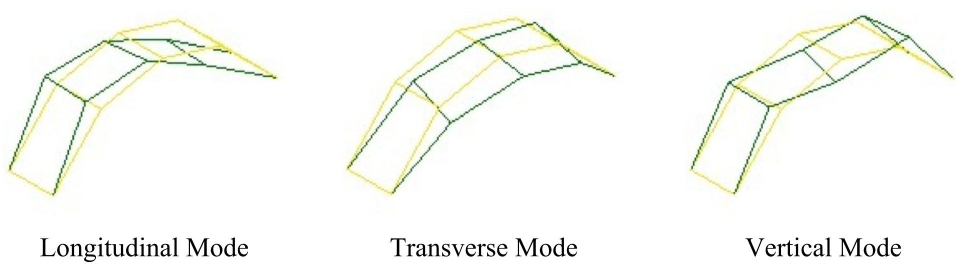

Fig. 14 Mode shapes of the models

MAC values calculated between numerical and experimental mode shapes obtained are also given in Table 6. As can be seen, there is a good correlation between each mode shape obtained from both models. To minimize the error and improve the accuracy, the initial FE model of bot models should be updated according to the experimental frequencies by changing some parameters included in the FE model.

Table 5 Natural frequencies of the models for the pre- and post-high-temperature test

Mode	Frequency (Hz)		
	Pre-test	Post-test	Difference (%)
Model 1			
1	60.46	33.26	44.99
2	87.40	45.24	48.24
3	127.20	68.10	46.46
Model 2			
1	68.40	30.55	55.34
2	100.70	51.42	48.94
3	127.30	67.86	46.69

4.2 Model updating procedure

The primary objective of FE model updating is to refine computational models by adjusting their parameters to better match experimental data such as dynamic characteristics, thereby improving their accuracy and predictive capability. FE model updating is employed to refine uncertain parameters, such as material properties, boundary conditions, and geometrical features, enhancing the accuracy of computational models. The pivotal stage in the model updating procedure is the selection of uncertain parameters for the finite element (FE) model.

It is known that the material properties, in particular the elasticity modulus of masonry structures, are challenging tasks due to the non-homogeneous nature of the structures. As previously mentioned, codes and prior studies have proposed significantly varied coefficients for calculating the elastic modulus of masonry. Therefore, the elastic modulus was selected as an uncertain parameter, and manual model updating procedure was practised by trial and error to obtain the final elasticity modulus. The acceptable limit value between the experimental and numerical natural frequency value was selected as 5–10%. The flowchart of the FE model updating procedure is given in Fig. 17. The initial modulus of elasticity was reduced by 23%. The final value was 2300 MPa. The final material properties and comparison of the dynamic characteristics of the

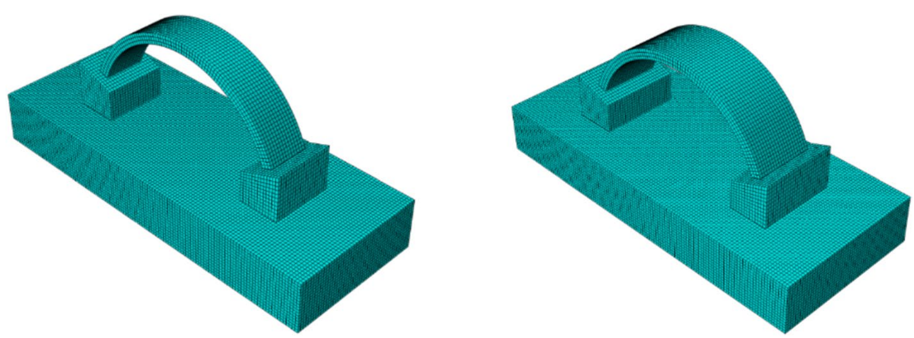

Fig. 15 FE models of both laboratory models

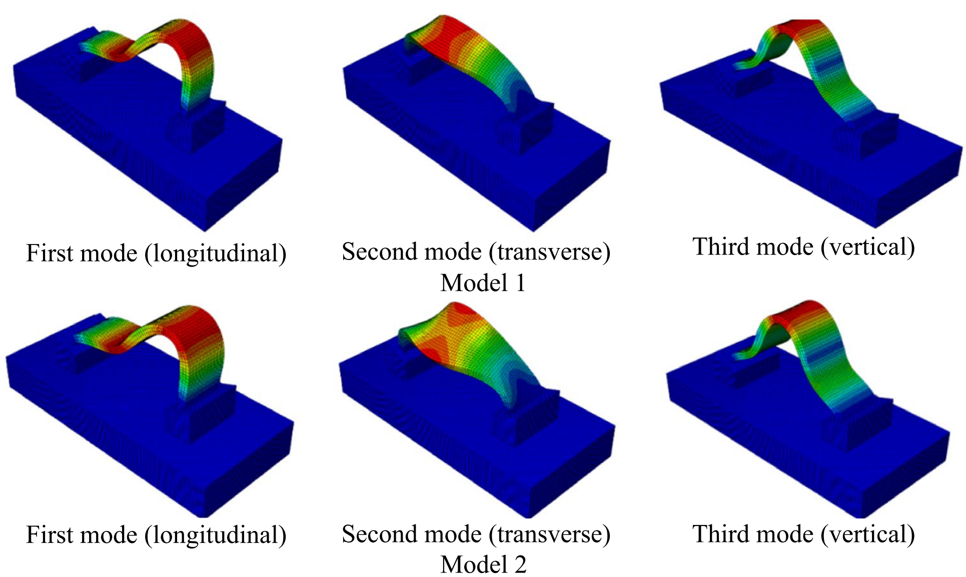

Fig. 16 First three numerical mode shapes for the initial FE models

Table 6 Numerical and experimental dynamic characteristics

Mode	Frequency (Hz)			
	Initial FE model	Experimental	Diff. (%)	MAC (%)
Model 1				
1	72.32	60.46	19.62	86
2	93.37	87.40	6.83	90
3	142.00	127.20	11.64	82
Model 2				
1	72.50	68.40	5.99	90
2	116.60	100.70	15.79	94
3	142.20	127.30	11.70	86

Table 7 Final material properties of the models

Material properties	Element		
	Foundation	Arch pillar	Masonry arch
Elasticity modulus (MPa)	36,000	36,000	2300
Poisson ratio	0.2	0.2	0.2
Density (kg/m^3)	2400	2400	2300

Table 8 Comparison of the numerical and experimental dynamic characteristics after the model updating procedure

Mode	Frequency (Hz)			
	Updated FE model	Experimental	Max. Diff. (%)	MAC (%)
Model 1				
1	63.45	60.46	4.95	86
2	82.08	87.40	6.09	96
3	124.60	127.20	2.04	84
Model 2				
1	63.63	68.40	6.97	92
2	102.50	100.70	1.79	95
3	124.90	127.30	1.89	88

models are illustrated in Tables 7 and 8, respectively. As can be seen in Table 8, the maximum differences between the two was decreased to below acceptable limit value. Note that the updated FE model is more representative of the current behaviour of the two models.

4.3 FE analyses results for the post-elevated temperature

FE models were constituted to obtain the dynamic characteristics of the models exposed to a high temperature of 600 °C. The material properties of the models with

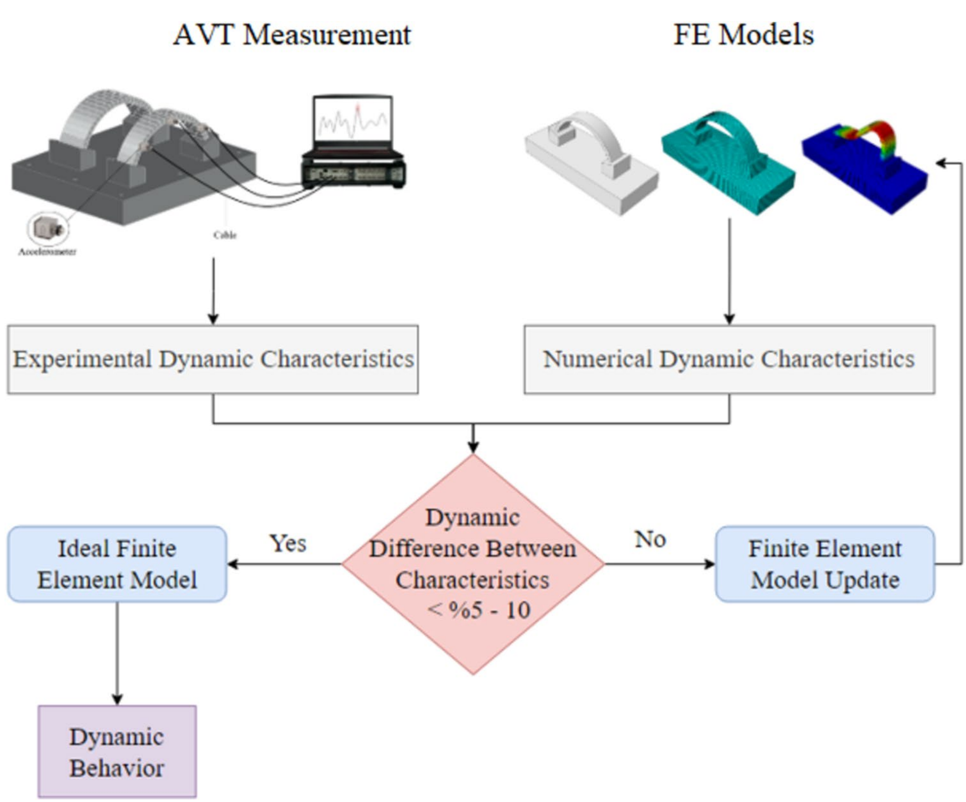

Fig. 17 Chart for the updating procedure

Table 9 Material properties of the FE models at 600 °C

Material properties	Element		
	Foundation	Arch pillar	Masonry arch
Elasticity modulus (MPa)	8600	8600	690
Poisson ratio	0.2	0.2	0.2
Density (kg/m^3)	2238	2238	2099

Table 10 Comparison of the numerical and experimental dynamic characteristics after exposure to a high temperature of 600 °C

Mode	Frequency (Hz)			
	Experimental	Updated FE model	Diff. (%)	MAC (%)
Model 1				
1	33.26	34.50	3.59	91
2	45.24	44.78	1.03	86
3	68.10	67.89	0.31	81
Model 2				
1	30.55	32.66	6.46	86
2	51.42	52.96	2.91	92
3	67.86	64.22	5.67	84

increasing temperature should be identified for thermal analysis. The boundary conditions for the previous FE models were also considered. The material characteristics were adjusted using data collected from material tests. According to EN 1992–1-2 [23], the density of concrete subjected to a temperature of 600 °C was determined to be 2238 kg/m^3. Bastami et al. [24] proposed equations to express changes in the elasticity modulus of concrete under the effects of elevated temperatures. Based on this information, the elasticity modulus of concrete at 600 °C was computed to be 8600 MPa. The density of the masonry was determined to be 2099 kg/m^3 based on the material tests. To determine the elasticity modulus of masonry samples, various studies and codes proposed an approach that correlates the compressive strength with the elasticity modulus of masonry. The standard method involves determining the elasticity modulus by multiplying the masonry's compressive strength by coefficients varying from 300 to 1000 [25]. The comprehensive strength of the masonry decreased by approximately 65–70% after exposure to 600 °C (see Table 3 and Table 4). Thus, the elasticity modulus of the masonry in the FE models subjected to elevated temperatures was determined by decreasing the value obtained for the updated FE models at room temperature by 70%. Table 9 presents the final material properties of the FE models at the 600 °C. Table 10 shows the dynamic characteristics obtained and their comparison with the experimental ones. As can be seen, the difference between both methods was acceptable with a value of 3.59% for Model 1 and 6.46% for Model 2. Also, the MAC values indicated that the numerical and experimental mode shapes are similar. Finally, it can be concluded that these models can be used for the further thermal analysis taking into account different parameters.

Structural elements exposed to high temperatures may experience additional stresses due to temperature changes, thermal expansions, and reductions in material strength, potentially leading to damage. This raises the question of how such potential damage might affect the dynamic characteristics of the structure. This issue has been investigated by incorporating thermal-stress analyses conducted after the validation process into the study. The research focused on finite element analyses of Model 1. To precisely capture the stress effects, a detailed solid finite element model of Model 1 was constructed, accurately reflecting the laboratory setup, including the arch, support legs, and model foundation. The analysis process began with a thermal-transient heat transfer analysis. The nodal temperatures obtained from this analysis were then used to perform a thermal-structural analysis. The stress values obtained were then used as initial conditions for modal analysis, aimed at assessing the impact of these stresses on the dynamic characteristics of the model. When comparing the dynamic characteristics of the model both with and without stress effects, it became apparent that the additional stresses had negligible impact on the natural frequency values. Considering the extensive computational demands of thermal-stress analyses and the negligible effect of stress impacts, these were not factored into the parametric analyses carried out in this study (Table 11).

4.4 Multiple analyses with variable parameters

This section presents the change in numerical dynamic characteristics with different parameters, taking into account fire

Table 11 Comparison of the numerical dynamic characteristics of the updated FE model of Model 1 after exposure to 600 °C: with and without additional stresses

Mode	Frequency (Hz)				
	Stresses excluded	Diff. (%)	Pre-heating condition	Diff. (%)	Stresses included
1	34.50	45.63	63.45	43.26	36.00
2	44.78	45.44	82.08	45.58	44.67
3	67.89	45.51	124.60	43.54	70.35

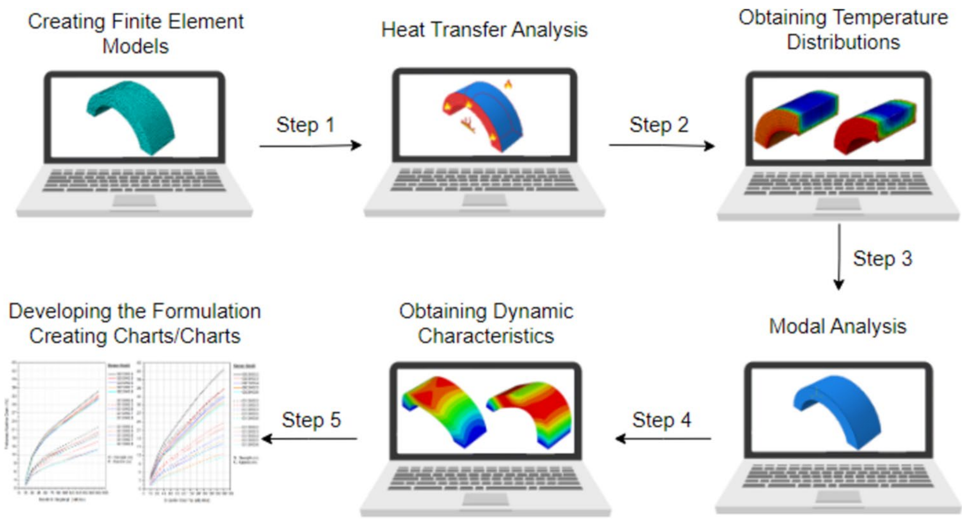

Fig. 18 The flowchart taken into account during developing of formulation and flowchart

effects. For this aim, numerous multiple heat transfer analyses with modal analyses were carried out to obtain the comprehensive data pool. Utilizing this data set, the formulations and graphical charts were developed. By examining how variations in these arch dimensions affect the dynamic characteristics of the structure under fire conditions, researchers can gain insights into optimizing arch design for enhanced performance and safety in such scenarios. Figure 18 presents the flowchart of the procedure.

The FE analyses were carried out for the arch with different geometries and fire impact scenarios (temperature histories). Table 12 shows the characteristics of the arches considered in the analyses. As can be seen, the arch span, arch height, arch width, and arch thickness were considered as an arch dimension. In addition, the temperature history, which denotes the duration of exposure to fire, was considered in the analysis. Heat transfer analyses were practised to determine temperature distributions within arch elements subjected to elevated temperatures, such as those occurring during a fire. The ISO 834 [26] standard temperature–time curve, spanning a 180-min period, was utilized for these analyses. A total of 13 distinct cases of the temperature history parameter were examined. These cases corresponded to exposure times of 0, 15, 30, 45, 60, 75, 90, 105, 120, 135, 150, 165, and 180 min. By exploring these varied exposure durations, researchers aimed to understand how different time intervals of fire exposure impact the dynamic behaviour and structural response of the arch elements.

4.5 Heat transfer analysis

It effectively conveys that to understand the dynamic behaviour of masonry arches under high temperatures, such as those experienced during a fire, it is essential to analyse the temperature distributions across the arch cross sections. This process involves conducting heat transfer analyses to determine the temperatures at all nodes on the finite element models representing the arch. FE models were employed in the heat transfer analysis of 450 arches, whose dimensions are detailed in Table 12. These models were generated using the ABAQUS software. Figure 19 shows a solid model of a 1–0.4–0.5–0.2 arch. The DC3D8 volumetric element with eight nodes was used for the heat transfer analysis.

In heat transfer analysis, the values of the thermal properties (thermal conductivity and specific heat) and density of the masonry material corresponding to certain temperatures were used. While thermal conductivity (k), one of the properties used in heat transfer analysis, expresses the ability

Table 12 Arch dimensions considered in multiple analyses

Group	Arch dimensions (m)										
	Span (s)	Height (h)		Width (w)			Thickness (t)				
1	1–3	$\frac{s}{2}$	$\frac{s}{2}\times 0.8$	0.5	1.0	1.5	0.2	0.3	0.4	0.5	0.6
2	4–7						0.4	0.5	0.6	0.7	0.8
3	8–11						0.6	0.7	0.8	0.9	1.0
4	12–15						0.8	0.9	1.0	1.1	1.2

The different arch dimensions to be analysed within the scope of the study are expressed as s–h–w–t (span–height–width–thickness). For example, the smallest and largest sized arches are expressed as 1–0.4–0.5–0.2 and 15–7.5–1.5–1.2, respectively

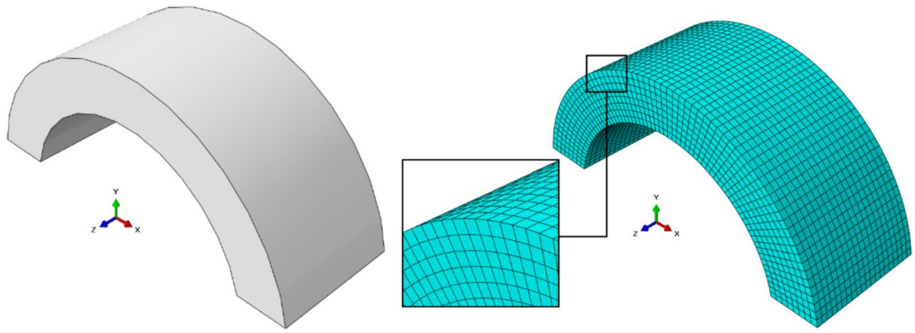

Fig. 19 Arch model for the heat transfer analysis

Table 13 Thermal material properties to be used in the FE model for heat transfer analysis of arch models

Temperature (°C)	Thermal material properties	
	Specific heat coefficient (J/kgK)	Thermal conductivity coefficient (W/mK)
0	900	2.000
20	900	1.951
100	900	1.766
115	1470	1.732
200	1470	1.553
300	1000	1.361
400	1050	1.191
500	1100	1.042
600	1100	0.915
700	1100	0.809
800	1100	0.724
900	1100	0.661
1000	1100	0.619
1100	1100	0.599
1200	1100	0.600

of a material to transmit heat, specific heat (c) represents the amount of energy required to raise the temperature by one unit. In the literature, experimental data on the thermal properties of masonry materials are limited. It is also widely accepted that masonry and concrete have comparable thermal properties. This is due to the similarities between the building materials [27]. For this reason, within the scope of the study, the variation of thermal material properties such as thermal conductivity and specific heat of masonry arches built using stone and mortar, depending on temperature, was calculated using the equation set out in the EN 1992–1-2 standard. Table 13 presents the thermal material properties used in the FE analysis. The density values obtained from the wall samples under the different temperature values (refer to Tables 3 and 4) were considered in the FE analyses. The meshing size selected was 0.025–0.065 m and the solid elements varied between 10,720 and 233,280. Figure 19 shows the FE model of the arches for the 1–0.4–0.5–0.2 cases.

During the heat transfer analyses, the temperature distributions at the arch models were determined by solving the heat conduction problem in the transient regime. The thermal conditions of the surfaces forming the boundaries of the model have an important influence on the solution of the problem. Here, the initial temperatures of the arch models obtained in different size cases were defined as 20 °C (room temperature) and heat transfer analyses were carried out for the cases where the fire affected the bottom and side surfaces of the arch models. In the transient regime, thermal analyses were conducted on arch models of varying sizes exposed to fire. These models were subjected to the ISO 834 temperature–time curve. The analyses consisted of a total of 12 steps, each with 15-min time intervals, covering the entire 180-min fire duration. Finally, the temperature values of all the nodal points on the FE model of the arches and the temperature distributions along the cross sections of the arch models were determined. Figure 20 also presents the temperature distributions formed at the end of certain time intervals (30, 60, 90, and 120 min) on the cross section of 1–0.4–0.5–0.2 cases. Due to the exposure of the lower and side surfaces of the arch elements to heat, temperature differences have occurred at the nodal points in the direction of these surfaces. However, there was no temperature difference between the nodes in this direction, as there is no temperature effect on the top of the elements.

4.6 Modal analyses

After the heat transfer analyses, modal analyses were practised to fire-exposed models to obtain the dynamic characteristics. This approach ensures that the material properties are considered based on the temperatures corresponding to all nodes for the respective times. For this, the mesh size and geometric properties of the FE models used in both heat transfer analysis and modal analyses should be same. For

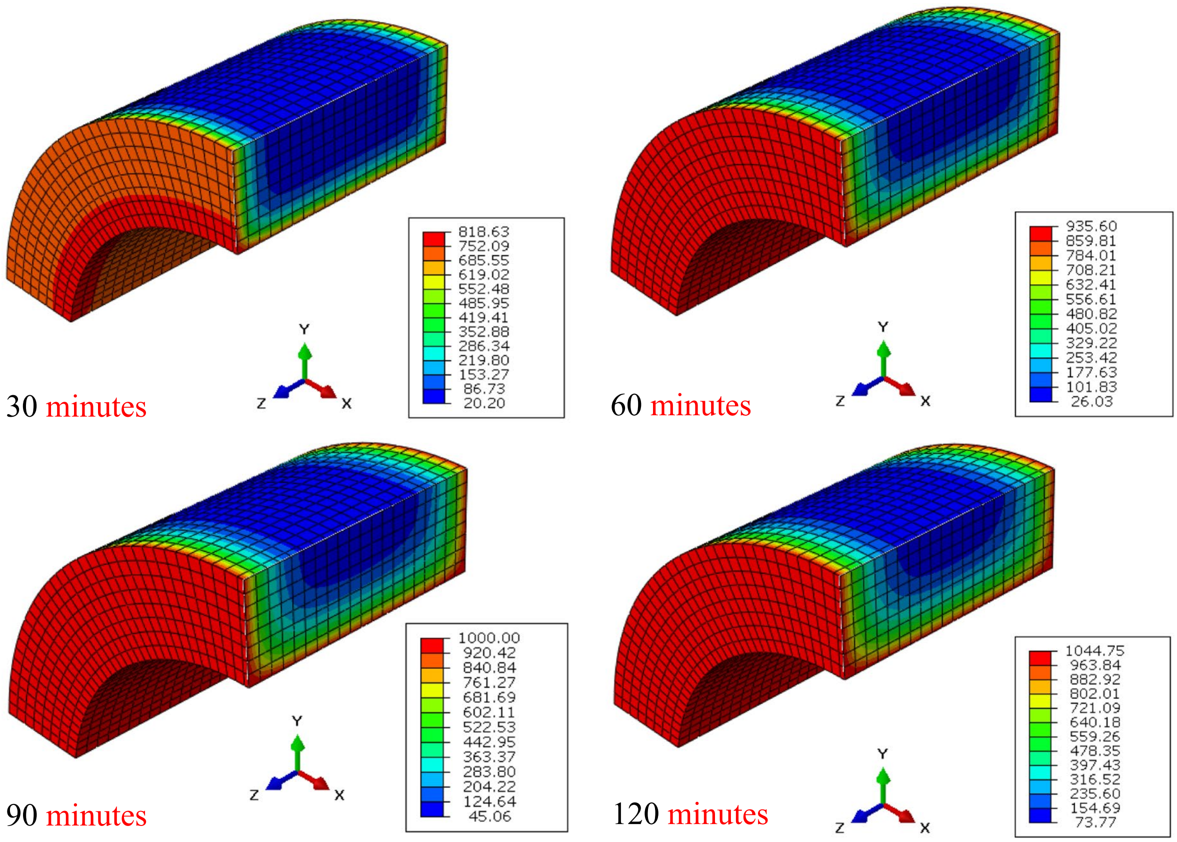

Fig. 20 Temperature distributions on the cross section of 1–0.4–0.5–0.2 cases exposed to elevated temperature

Table 14 Material properties used in the FE model for the modal analyses

Temperature (°C)	Material properties		
	Poisson ratio (-)	Density (kg/m^3)	Modulus of elasticity (MPa)
0	0.2	2302	2300
20	0.2	2302	2300
200	0.2	2235	2323
400	0.2	2124	1426
600	0.2	2099	690
800	0.2	2038	460
1000	0.2	1976	1

Table 15 Natural frequency changes with the increasing temperature histories

Temperature histories (min)	Natural frequencies (Hz)		
	First mode	Second mode	Third mode
0	104.48	122.79	188.90
15	100.07	117.78	182.47
30	93.23	109.28	171.51
45	88.55	103.28	163.64
60	85.27	99.71	158.61
75	82.07	96.17	153.45
90	79.00	92.90	148.63
105	75.93	89.63	143.78
130	72.90	86.21	138.67
145	70.09	82.92	133.83
160	67.49	79.77	129.19
175	65.03	76.79	124.30
180	62.72	74.14	120.18

the modal analysis using results from heat transfer analysis, element type of C3D8R was used. In the analyses, while the variation of the elasticity modulus and density of the arches with temperature was taken into account, the variation of the Poisson ratio with temperature was ignored (Poisson ratio was considered as 0.2 for all cases). For the temperature-dependent density value of masonry arches, the values set out in Sect. 2 were used. The elasticity modulus of the arches used in the FE analyses was determined by updating the procedure in accordance with the AVT conducted under laboratory conditions at temperatures of 20 °C and 600 °C.

As detailed above, compressive strength tests to wall samples were performed. As known, a direct relationship can be established between the compressive strength and elasticity modulus. Hence, elasticity modulus values corresponding to other temperature values (200 °C, 400 °C, 800 °C, and 1000 °C) were determined by extrapolating from the observed changes in compressive strength. Table 14 presents the material properties for the modal analyses with the different temperature values.

The duration of exposure to standard fire was determined for intervals ranging from 15 to 180 min. Table 15 presents the changing of natural frequencies with the increasing temperature histories. It is evident that increasing the temperature exposure time of the respective arch element leads to a decrease in the natural frequency values of the element. The first three natural frequencies decreased as 39.97%, 39.62%, and 36.38%. Figure 21 shows the mode shapes obtained. The mode shapes for both cases (pre- and post-fire) are similar.

4.7 Developing formulation and graphs/charts

Heat transfer analyses were conducted on 450 arches of varying sizes, followed by 5850 modal analyses based

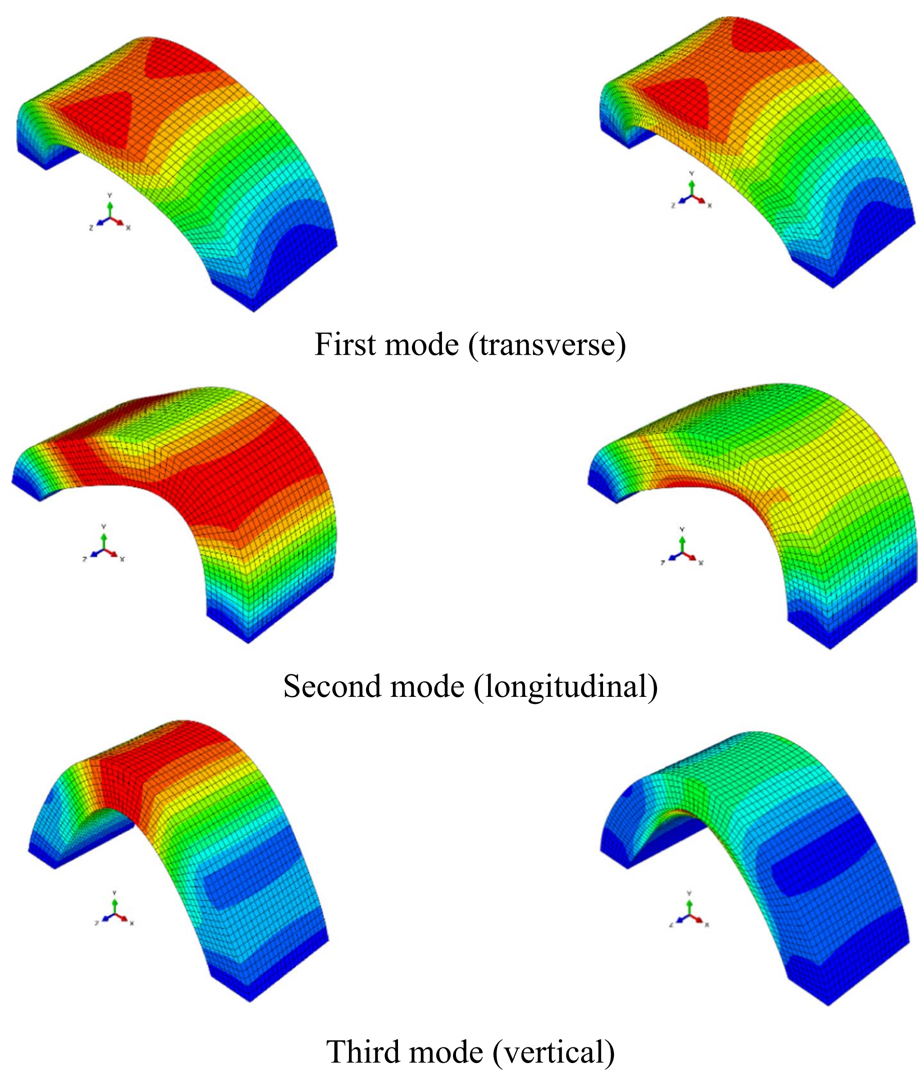

Fig. 21 Mode shapes for both pre- (left side) and post- (right side) fire cases

on the outcomes of these analyses. Consequently, a substantial repository of data was generated from all these analyses. Utilizing this data repository, the objective is to promptly ascertain variations in the dynamic characteristics of these arches with a temperature history, formulate findings, and generate graphs/charts to discern stiffness alterations and damage. The formulation was developed by conducting regression analysis to determine the natural frequency values of the first mode for arches of various sizes and temperature histories.

The independent variables are interconnected and not entirely independent of each other. The relationships between the dependent and independent variables are not necessarily functional, and the values of the independent variables may vary among themselves. Such non-functional relationships between variables are often represented with mathematical expressions, such as regression equations [28]. Equation 1 presents the function used in the study.

$$y_{Exp} = w_0 + exp\left(w_1 + w_2x_1 + w_3x_2 + \cdots + w_{n+1}x_n\right) \quad (1)$$

In these equations, w_n represents the regression coefficients, x_n represents the independent variables, and y_{Exp} represents the frequencies of the first modes of the arches, which depend on the temperature histories and dimensions.

Given the challenge of modelling extreme values within the data set, all data pertaining to both the dependent and independent variables were normalized using Eq. 2. This normalization process aims to facilitate modelling, minimize the impact of varying dimensions, and yield more effective results [29].

$$X_n = \frac{X_i - X_{min}}{X_{max} - X_{min}} \times a + b \quad (2)$$

Here, X_n is the normalized value, X_{min} is the smallest value, and X_{max} is the largest value. In this study, the a and b coefficients were chosen as 0.8 and 0.1, respectively. Thus, all data used in the modelling were normalized between 0.1 and 0.9.

IBM SPSS statistics 25 software was used to obtain the regression coefficients. The coefficients were used and the model prediction results (f_{RA}) were calculated for the data set (f_{FE}). Equation 3 was derived by substituting the calculated coefficients from Eq. 1.

$$\begin{aligned} f_1 &= 0.0117 + exp(0.779 + 10.277S - 25.684H \\ &+0.823W - 0.949T - 0.001t) \end{aligned} \quad (3)$$

In this exponential function with five variables, S, H, W, and T represent the arch span, height, width, and thickness (m), respectively. Also, t refers to the exposure time (min). The scatter plot of the predicted values in the regression analysis and the calculated values in the FE analysis are given in Fig. 22.

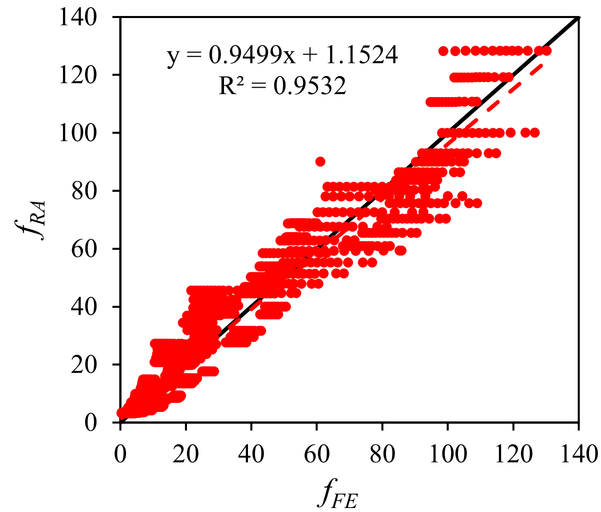

Fig. 22 The scatter plot of the predicted values in the regression analysis and the calculated values in the FE analysis

In addition to the formulation proposed, the presented graphs depict the reduction rates in the natural frequency values of the first mode, which vary depending on the temperature histories of arches with different dimensions exposed to elevated temperatures. These graphs/charts are based on the results of 5850 analyses. In the analyses, different parameters such as spacing, height, width, and thickness were considered. The graphs/charts were developed for the width parameters of 0.5, 1.0, and 1.5 m with different span parameter varying between 1.0 and 15 m with 1.0 m intervals, and five thickness parameters varying between 0.2 and 1.2 m (Figs. 23, 24, 25, 26, 27, 28, 29, 30, 31, 32, 33, 34, 35, 36, 37). The decrease rates of the first natural frequency value, depending on the temperature history, are illustrated by comparing the conditions of 15 different arches with the same spacing, but without any temperature histories. As the height of the arch increases, there is a transition from a flat arch to a semicircular arch. In this case, during the fire analyses, it was found that the rate of decrease in frequency values with increasing temperature was similar. Therefore, the height parameter was ignored in the process of developing the graphs/charts.

5 Conclusion

This study aims to present the changes in the dynamic characteristics of masonry arches exposed to elevated temperatures and to develop formulations and graphs/charts for practical application. The following conclusions are drawn from the study:

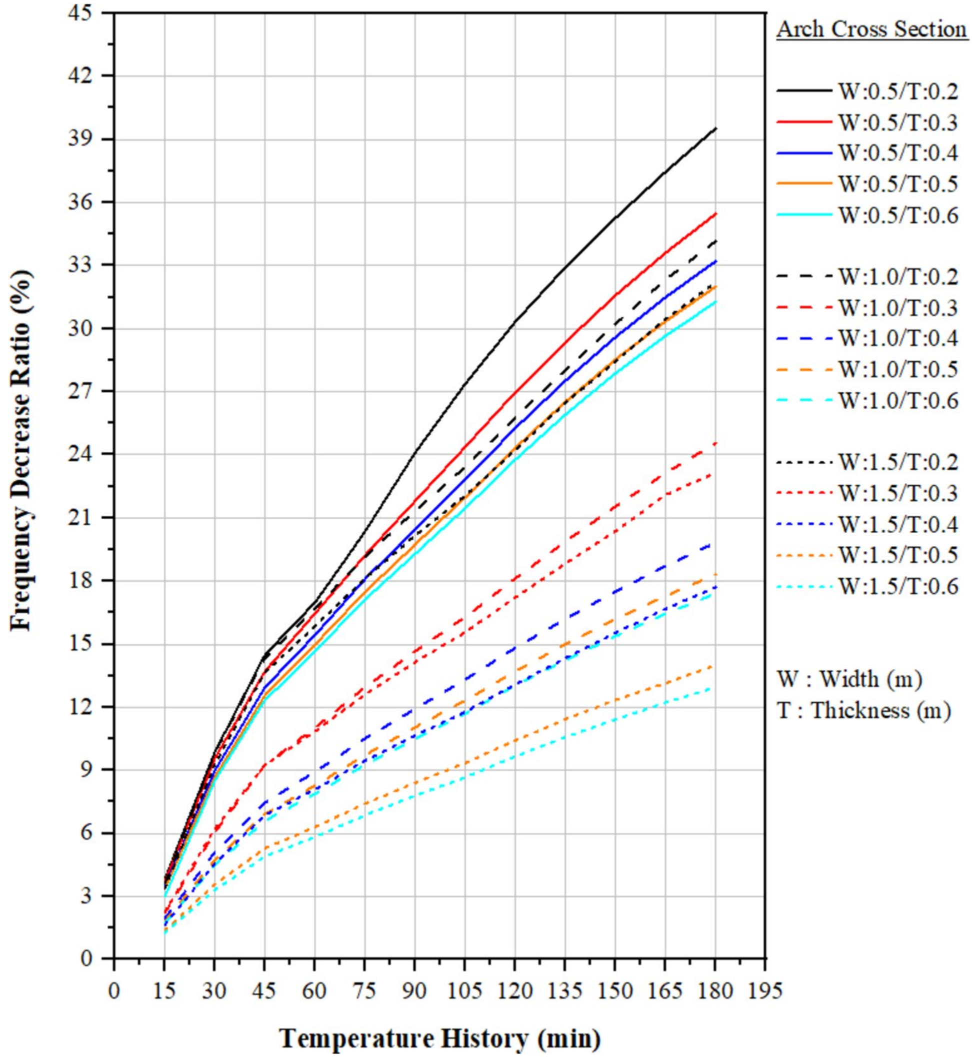

Fig. 23 Rate of decrease of natural frequencies with increasing temperature histories for the 1.0 m span and different cross sections

- The density of the wall samples decreased with the increasing temperature. Also, the compressive strength of the samples increased up to 200 °C, and started to decrease after 400 °C. The compressive strength of the samples decreased by approximately 72–78% at 800 °C.
- The mode shapes obtained were the same for the pre- and post-high-temperature test.
- The natural frequencies of arch models decreased sharply with increasing temperature histories.
- The modal updating procedure was effectively implemented to minimize the differences between the experimental and numerical results.
- During the heat transfer analysis, it was concluded that the mesh size plays an important role in accurately capturing the temperature distributions within the model.
- A formulation was developed to compute the first natural frequencies of the arch, which includes its geometric dimensions (span, height, width, and thickness) and the duration of exposure to temperature as key variables.
- Graphs/charts were presented showing reduction rates in the first natural frequency, which vary depending on the temperature histories of masonry arches with different dimensions exposed to elevated temperatures.
- The 20% decrease at the height parameter, considered in the analysis, led to an increase in the first natural frequency values of the arches with the same span, width, and thickness. Additionally, it was observed that the rate of decrease in the first natural frequencies of the

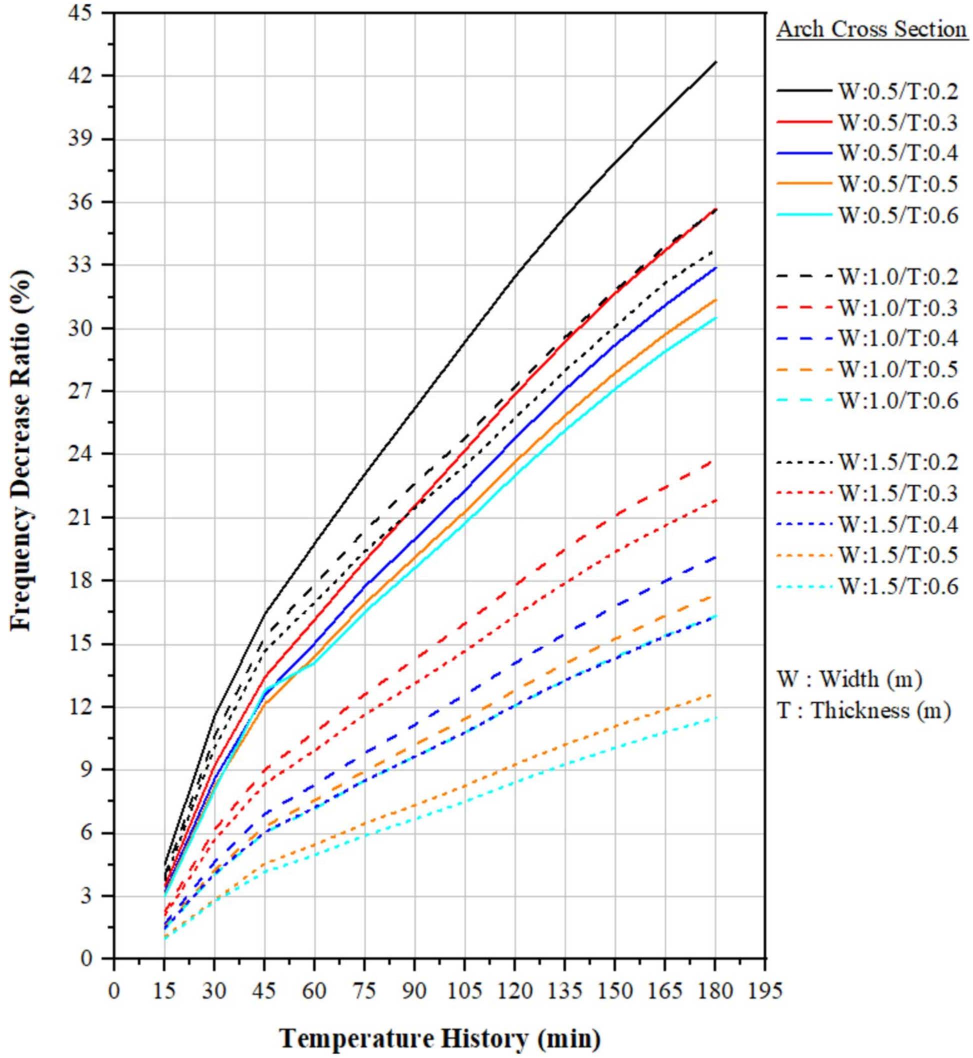

Fig. 24 Rate of decrease of natural frequencies with increasing temperature histories for the 2.0 m span and different cross sections

semicircular and flattened arches exposed to high temperature was similar.

- In arches with the same span, height, and thickness, an increase in the width parameter generally resulted in an increase in the natural frequency values corresponding to the first mode of the arches. However, the increase in the width parameter of these arches exposed to heat led to a decrease in the natural frequency reductions depending on the temperature history of the arches.
- In arches with the same span, height, and width, the increase in the thickness parameter generally caused a decrease in the natural frequency values corresponding to the first mode of the arches. In addition, the increase in the thickness parameter of these arches exposed to heat caused a decrease in the frequency of the arches depending on the temperature history.
- Finally, it was observed that the rate of decrease in the natural frequencies of arches exposed to high temperature was not significantly affected by changes in the span and height parameters, whereas increases in the width and thickness parameters decreased this rate.

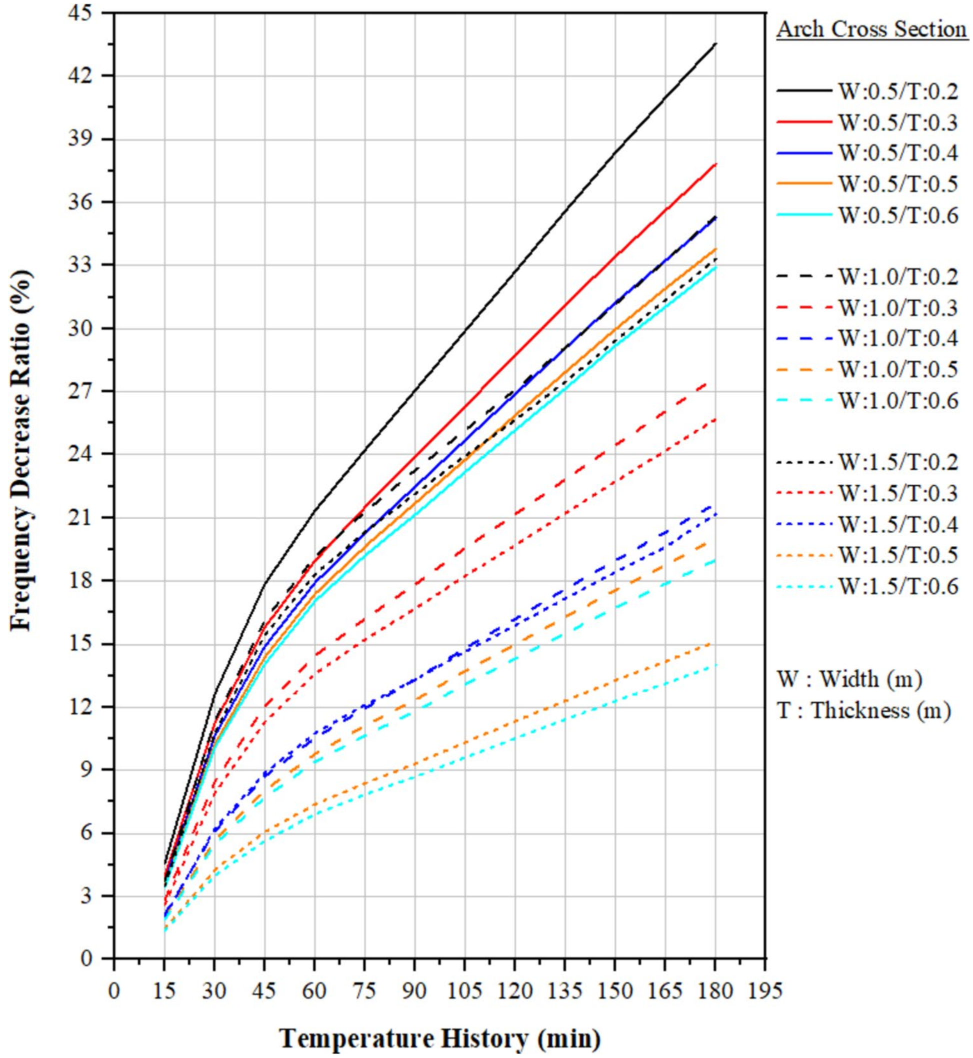

Fig. 25 Rate of decrease of natural frequencies with increasing temperature histories for the 3.0 m span and different cross sections

This study has observed that in masonry structures, the dynamic characteristics of arches, which are significant components, can be substantially affected following a potential fire, and efforts have been made to practically determine the post-fire usage conditions of these elements. With further research, the diversity of parameters considered in this study can be increased, thereby expanding the data pool. Additionally, the data pool can be enriched through similar studies that consider parameters related to different masonry building materials, various fire models, and surfaces exposed to fire. The need for extensive finite element analysis, prompted by the increase in parameters, can be efficiently managed without the use of a finite element program interface by integrating simple software based on prepared coding with batch processing methods. Moreover, to provide more precise data on the changes in properties of different masonry materials at high temperatures required for these analyses, the number of experimental studies addressing this issue should be expanded. Consequently, it should be ensured that the accuracy and reliability of the numerical results obtained are increased.

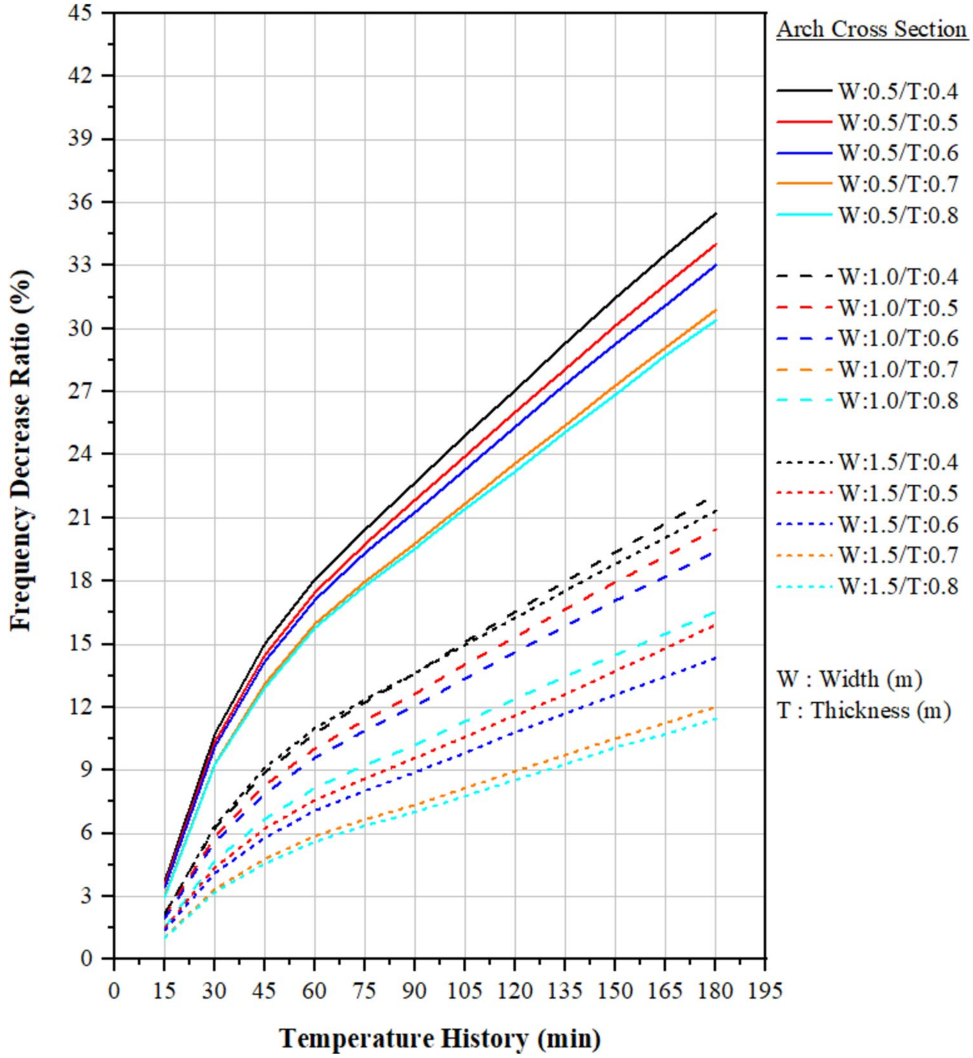

Fig. 26 Rate of decrease of natural frequencies with increasing temperature histories for the 4.0 m span and different cross sections

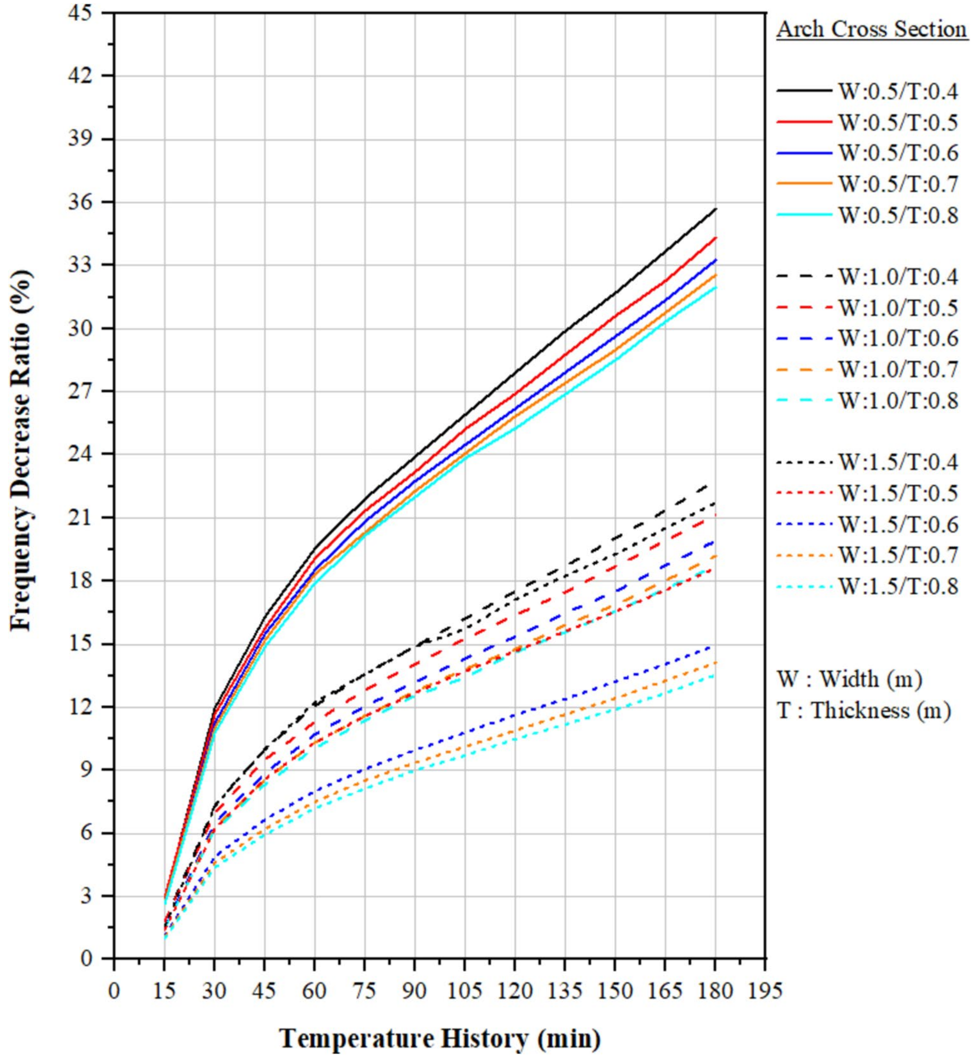

Fig. 27 Rate of decrease of natural frequencies with increasing temperature histories for the 5.0 m span and different cross sections

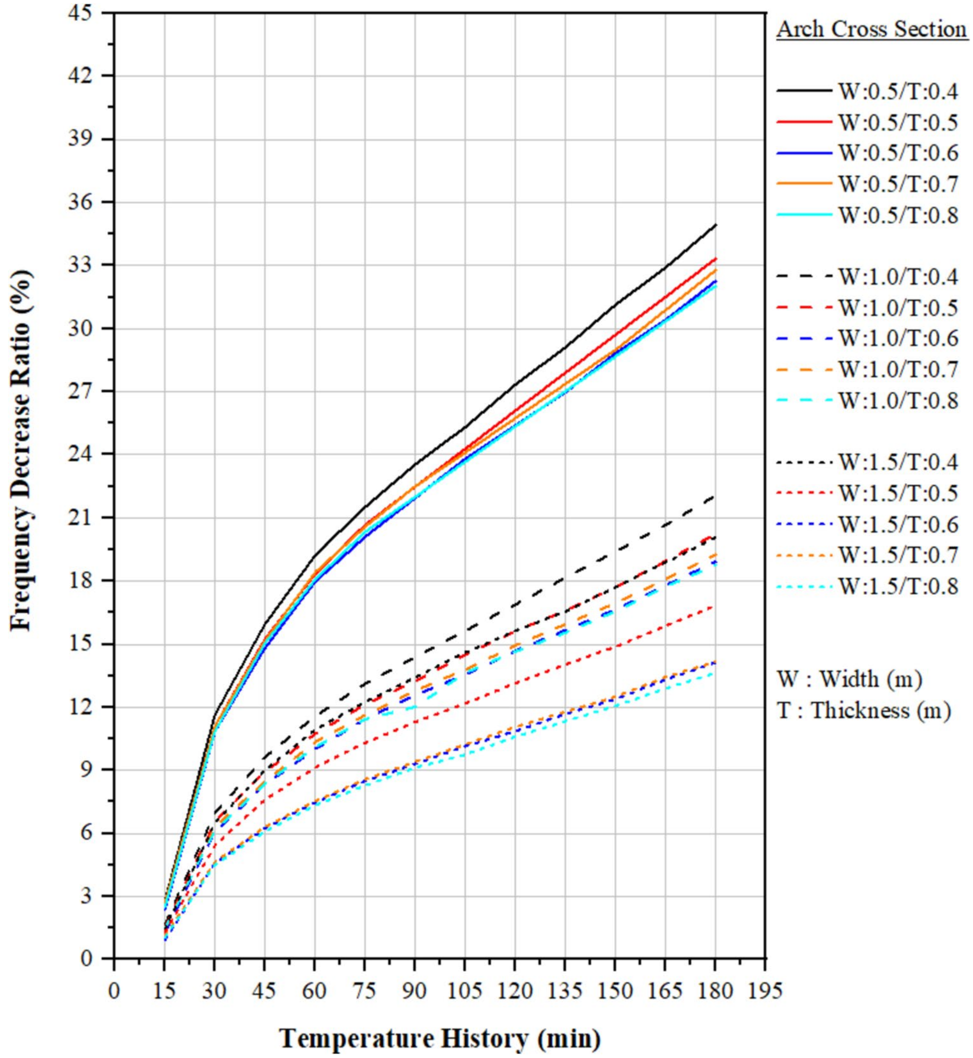

Fig. 28 Rate of decrease of natural frequencies with increasing temperature histories for the 6.0 m span and different cross sections

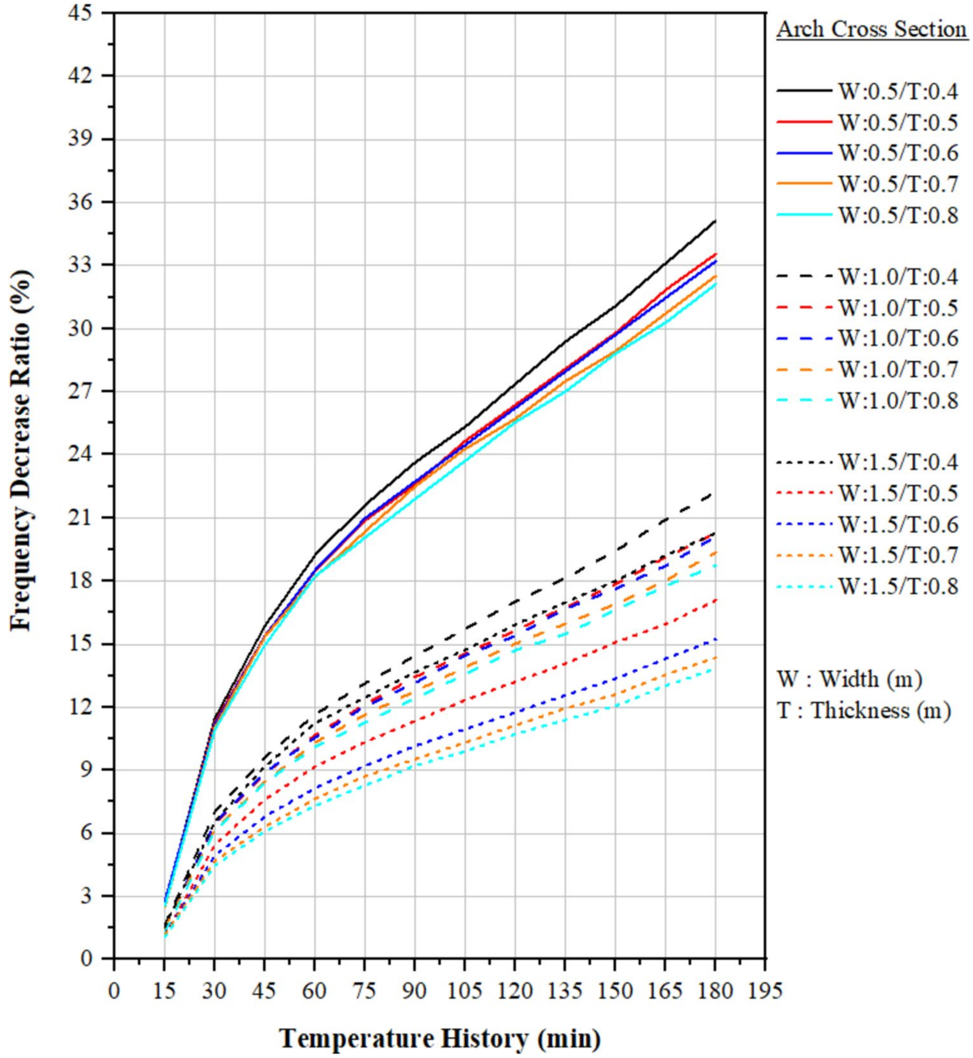

Fig. 29 Rate of decrease of natural frequencies with increasing temperature histories for the 7.0 m span and different cross sections

Fig. 30 Rate of decrease of natural frequencies with increasing temperature histories for the 8.0 m span and different cross sections

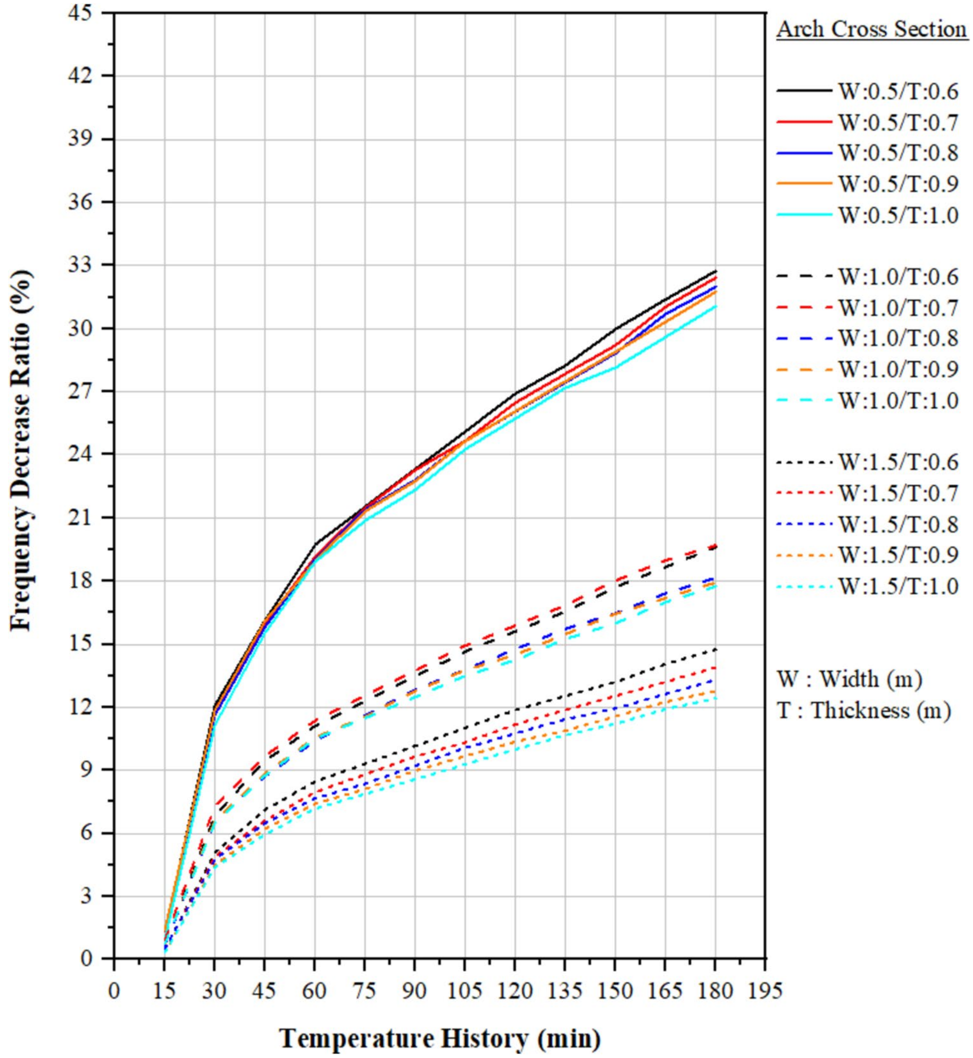

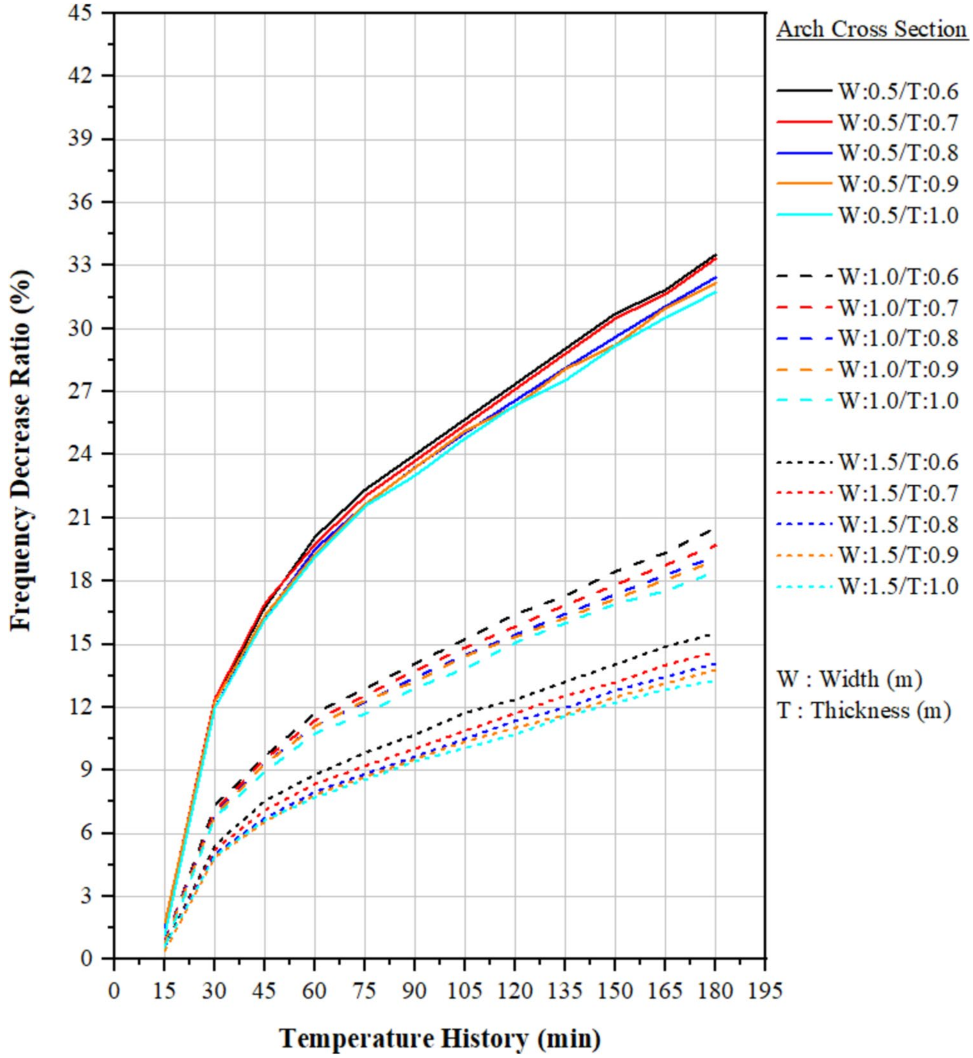

Fig. 31 Rate of decrease of natural frequencies with increasing temperature histories for the 9.0 m span and different cross sections

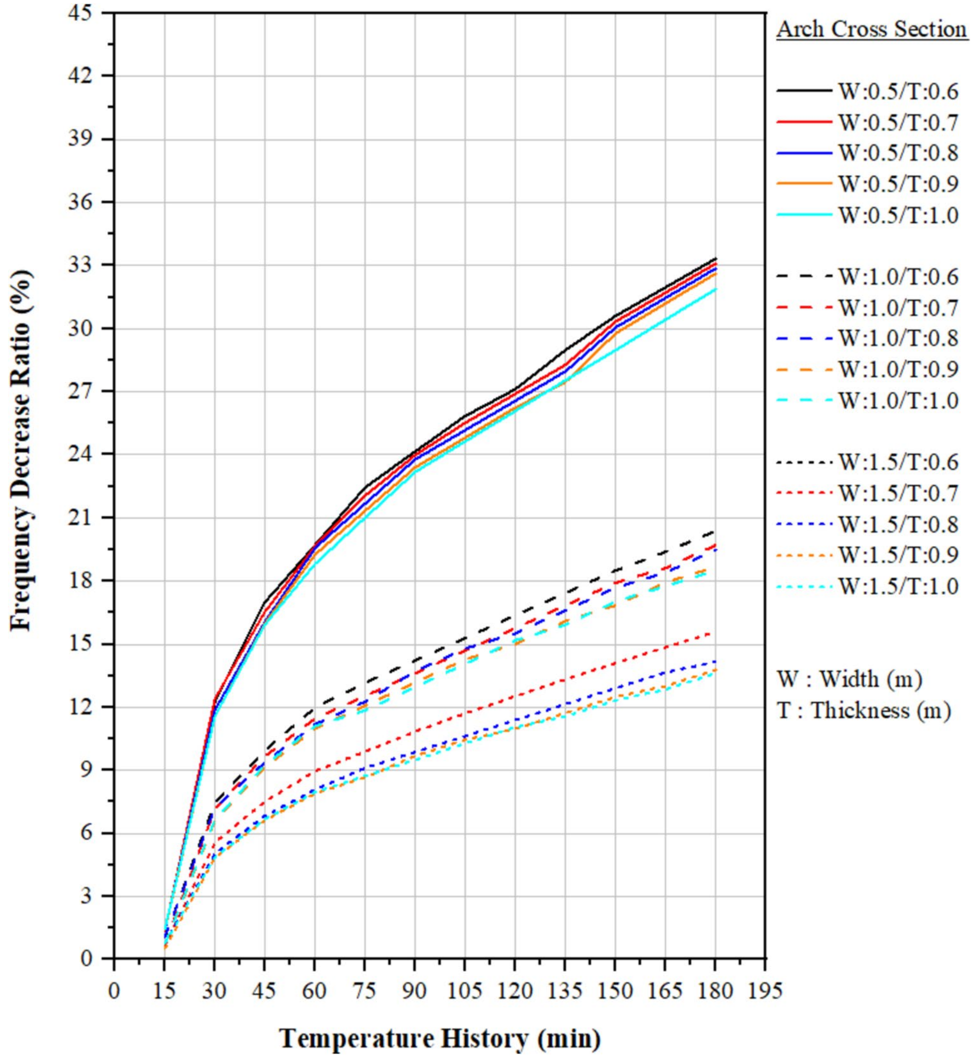

Fig. 32 Rate of decrease of natural frequencies with increasing temperature histories for the 10 m span and different cross sections

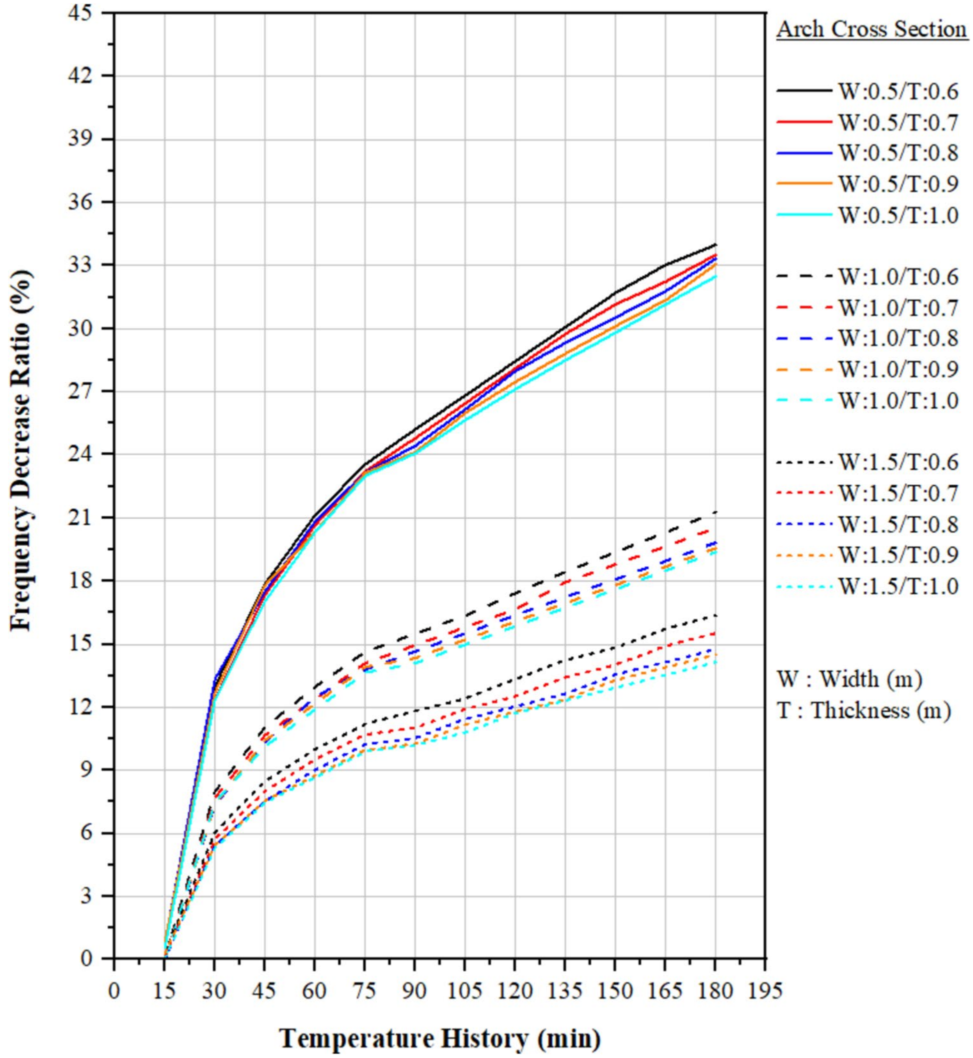

Fig. 33 Rate of decrease of natural frequencies with increasing temperature histories for the 11 m span and different cross sections

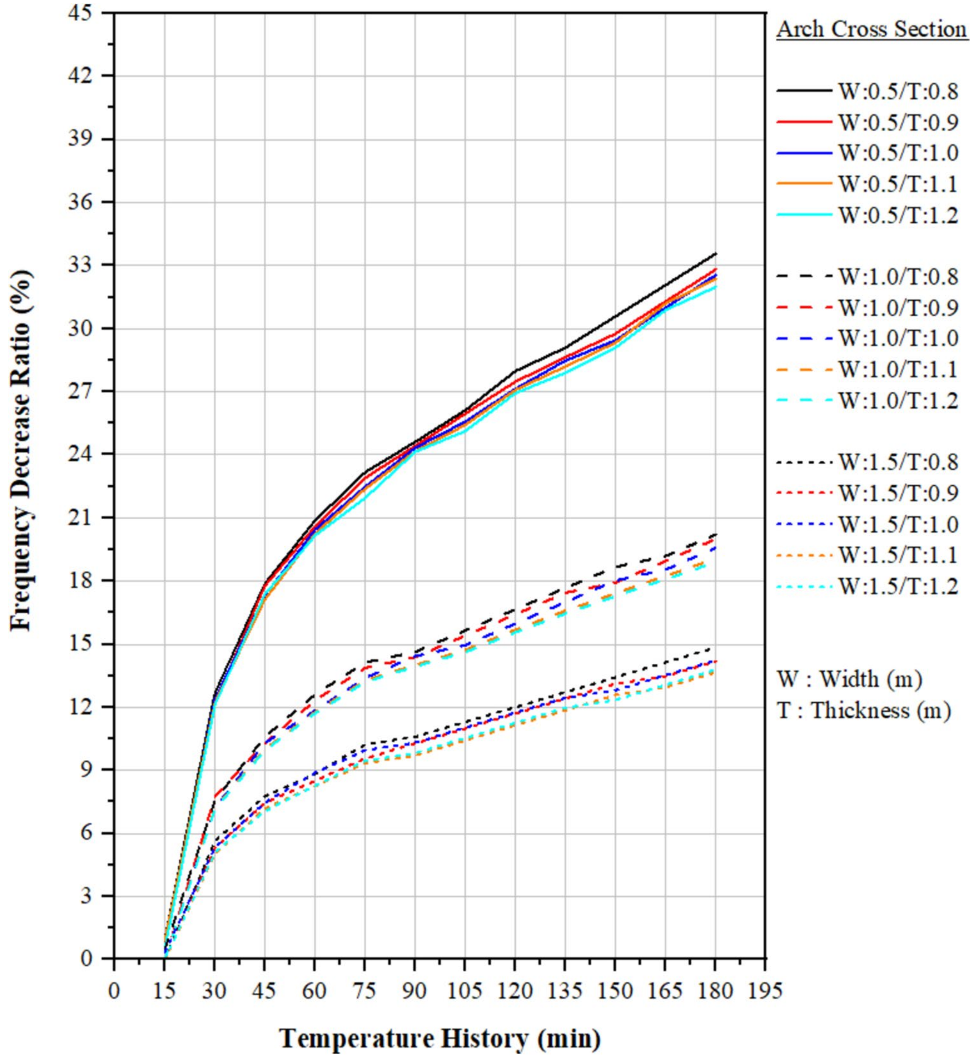

Fig. 34 Rate of decrease of natural frequencies with increasing temperature histories for the 12 m span and different cross sections

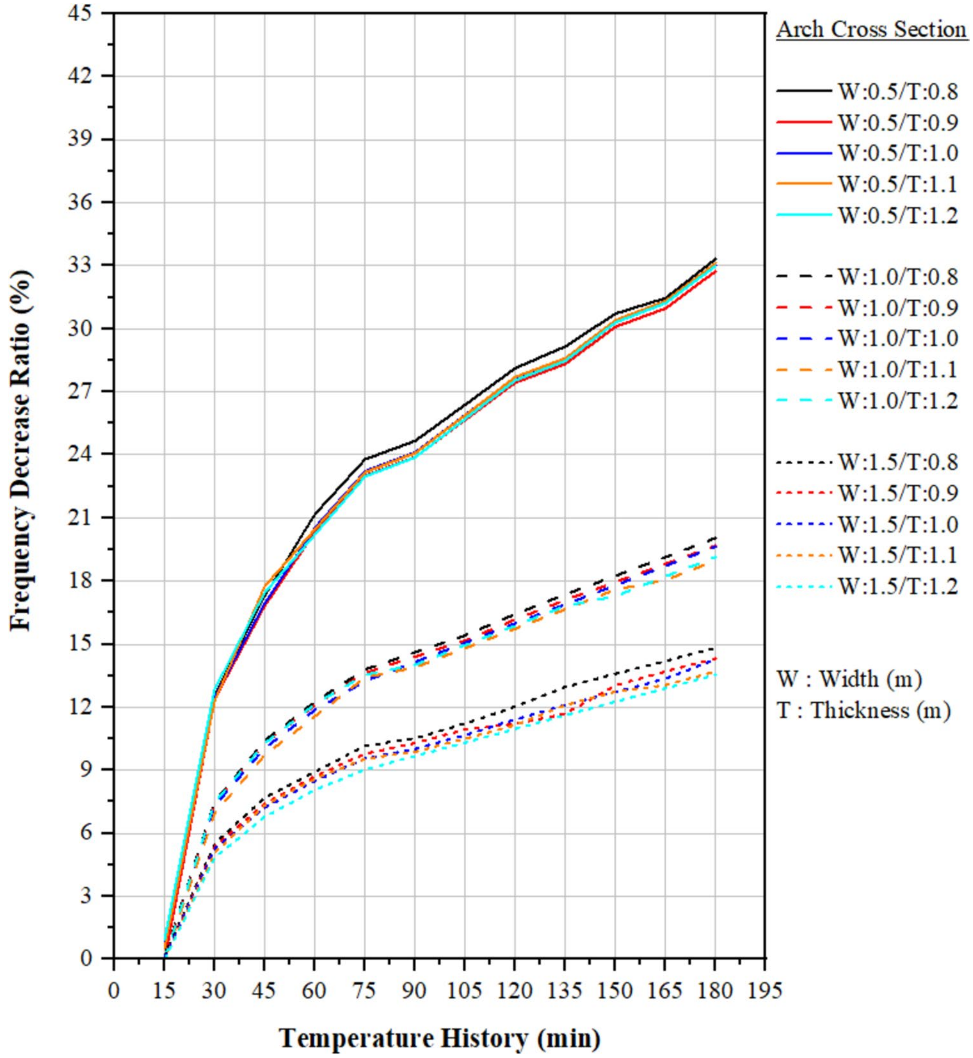

Fig. 35 Rate of decrease of natural frequencies with increasing temperature histories for the 13 m span and different cross sections

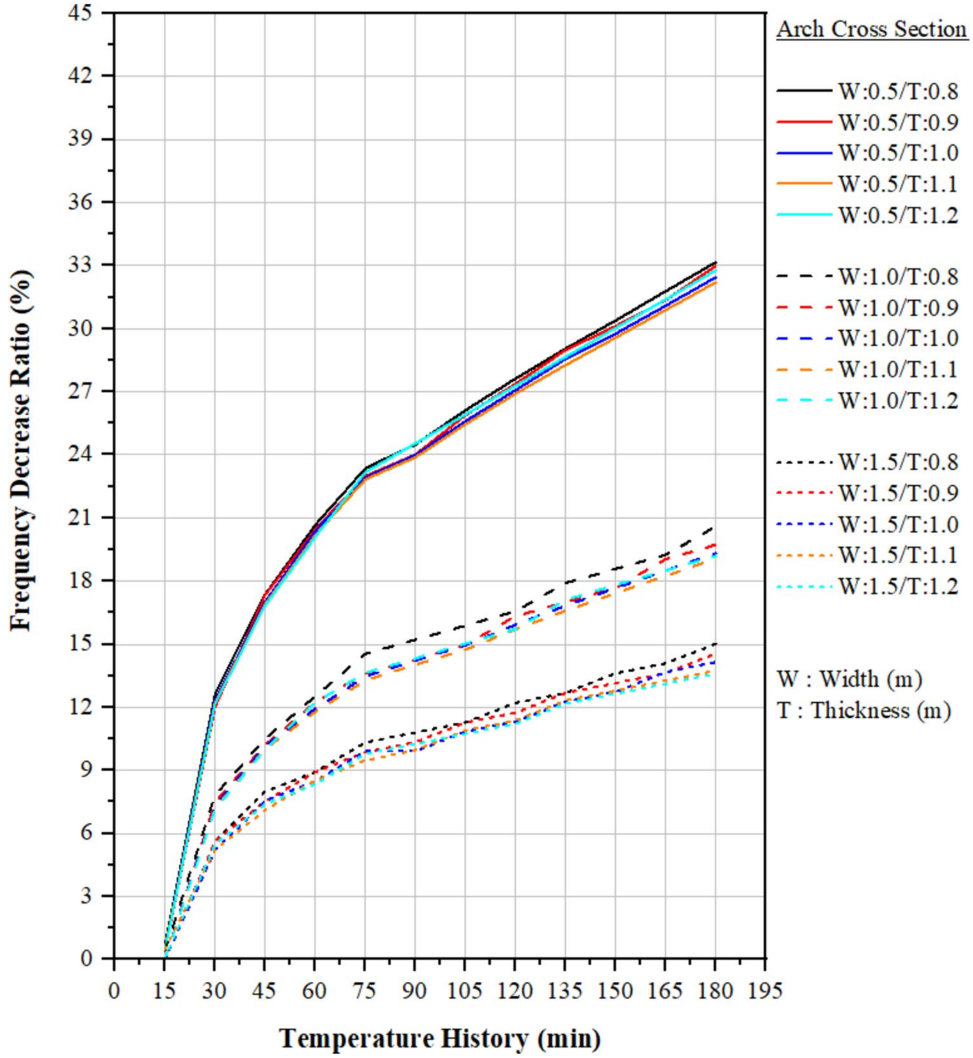

Fig. 36 Rate of decrease of natural frequencies with increasing temperature histories for the 14 m span and different cross sections

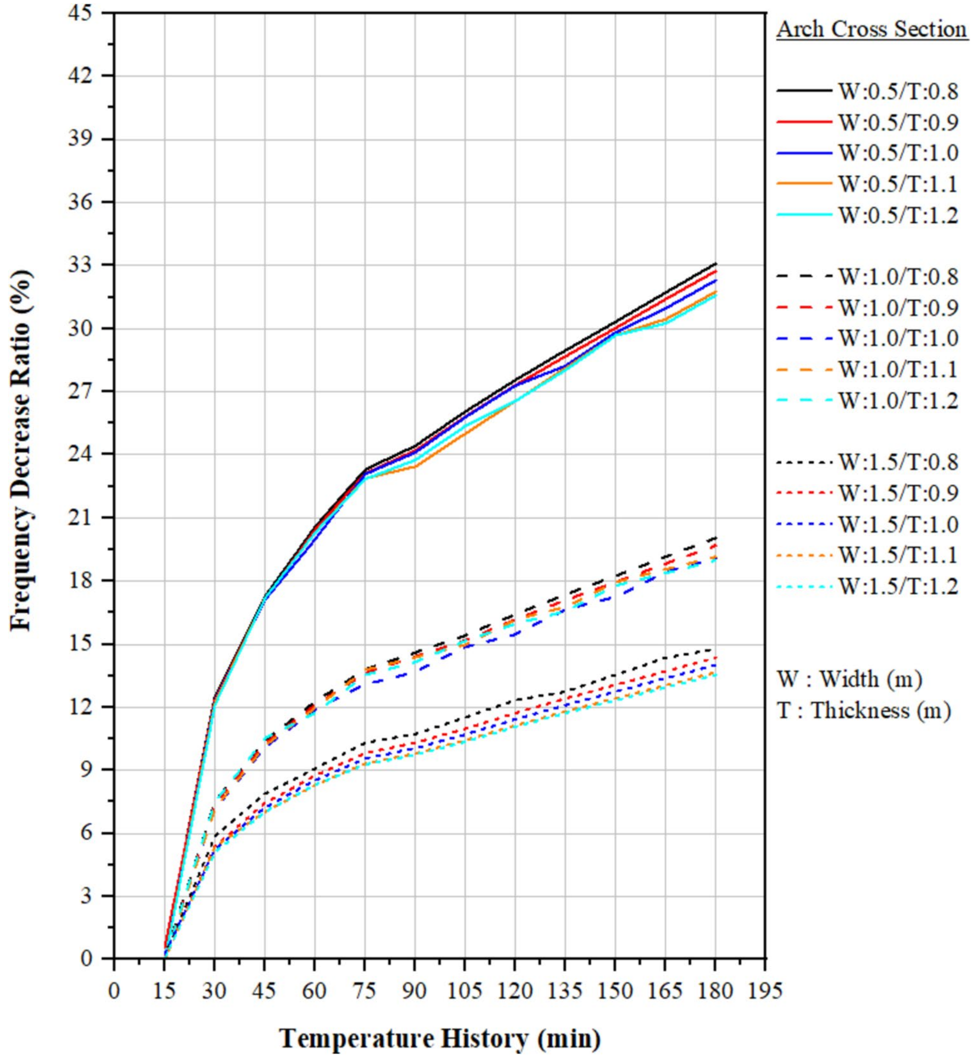

Fig. 37 Rate of decrease of natural frequencies with increasing temperature histories for the 15 m span and different cross sections

Acknowledgements The authors appreciate the infrastructure and collaborative framework provided by the Scientific and Technological Research Council of Turkey (TÜBİTAK; Grant No. 117M819) and the Karadeniz Technical University Scientific Research Projects Coordination Unit (BAP; Grant Nos. FBA-2018-7292 and FBA-2022-10509).

Data availability Data available on request from the authors.

Declarations

Conflict of interest We wish to confirm that there are no known conflicts of interest associated with this publication and there has been no significant financial support for this work that could have influenced its outcome.

References

1. Pirchio D, Walsh KQ, Kerr E, Giongo I, Giaretton M, Weldon BD, Ciocci L, Sorrentino L. Integrated framework to structurally model unreinforced masonry Italian medieval churches from photogrammetry to finite element model analysis through heritage building information modeling. Eng Struct. 2021;241:112439. https://doi.org/10.1016/j.engstruct.2021.112439.
2. Altunişik AC, Bayraktar A, Sevim B, Birinci F. Vibration-based operational modal analysis of the Mikron historic arch bridge after restoration. Civ Eng Environ Syst. 2011;28(3):247–59. https://doi.org/10.1080/10286608.2011.588328.
3. Votsis RA, Kyriakides N, Chrysostomou CZ, Tantele E, Demetriou T. Ambient vibration testing of two masonry monuments in Cyprus. Soil Dyn Earthq Eng. 2012;43:58–68. https://doi.org/10.1016/j.soildyn.2012.07.015.
4. Standoli G, Giordano E, Milani G, Clementi F. Model updating of historical belfries based on Oma identification techniques. Int J Archit Herit. 2021;15(1):132–56. https://doi.org/10.1080/15583058.2020.1723735.
5. Bayraktar A, Hökelekli E, Türker T, Çalik İ, Ashour A, Mosallam A. Window opening effects on structural behavior of historical masonry Fatih Mosque. Int J Archit Herit. 2019;13(4):585–99. https://doi.org/10.1080/15583058.2018.1447617.
6. Calayır Y, Yetkin M, Erkek H. Finite element model updating of masonry minarets by using operational modal analysis method. Structures. 2021;34:3501–7. https://doi.org/10.1016/j.istruc.2021.09.103.

7. Günaydın M, Demirkır C, Altunışık AC, Gezer ED, Genç AF, Okur FY. Diagnosis and monitoring of historical timber velipaşa han building prior to restoration. Int J Archit Herit. 2023;17(2):285–309.
8. Altunişik AC, Öztürk MM, Genç AF, Günaydın M, Kaya A, Akbulut YE, Sunca F. Dynamic characteristics changes of masonry arches exposed to elevated temperature. Constr Build Mater. 2024;418:135423.
9. ASTM C 1314–02a, Standard Test Method for Compressive Strength of Masonry Prisms, (2002). ASTM International, West Conshohocken, PA.
10. TS EN 1052–1, Methods of test for masonry—Part 1: Determination of compressive strength, (2000). Turkish Standards Institute (TSI), Ankara, Turkey.
11. PULSE. (2006). Analyzers and Solutions, Release 11.2. Bruel and Kjaer, Sound and Vibration Measurement A/S, Denmark.
12. OMA. (2006). Operational Modal Analysis, Release 4.0. Structural Vibration Solution A/S, Denmark.
13. ABAQUS. (2017). Dassault Systems Simulia Corporation, Providence, Rhode Island.
14. TS 500, Design and Construction Rules of Reinforced Concrete Structures, (2000). Turkish Standards Institute (TSI), Ankara, Turkey. (2000).
15. Guadagnuolo M, Aurilio M, Basile A, Faella G. Modulus of elasticity and compressive strength of tuff masonry: results of a wide set of flat-jack tests. Buildings. 2020;10(5):84.
16. FEMA-273, 1997. FEMA356 Nehrp Guidelines for The Seismic Rehabilitation of Buildings, Building Seismic Safety Council, Washington, D.C. USA
17. MSJC, 2002. Building code requirements for masonry structures, Masonry Standards Joint Committee (MSJC). ACI 530–02, ASCE 5–02, TMS 402, 2.
18. TEC, 2018. TEC2018 Turkey Earthquake Building Codes, Disaster and Emergency Management Presidency-Earthquake Department, Ankara.
19. CSA S304, 2004. Design of masonry structures, Canadian Standards Association (CSA), Mississauga, Canada.
20. EN 1996–1–1, 2005. Eurocode 6: Design of masonry structures - Part 1–1: General rules for reinforced and unreinforced masonry structures, European Committee for Standardisation (CEN), Brussels.
21. Crisafulli, F. J., Carr, A. J., & Park, R. (1995, November). Shear strength of unreinforced masonry panels. In Proceedings of the Pacific Conference on Earthquake Engineering (Vol. 3, pp. 77–86).
22. Drysdale RG, Hamid AA, Baker LR. Masonry Structures, Behavior and Design. Englewood Cliff: Prentice Hall Inc; 1994.
23. EN 1992–1–2, 2004. Eurocode 2: Design of Concrete Structures—Part 1–2: General Rules Structural Fire Design, European Committee for Standardisation (CEN), Brussels.
24. Bastami M, Aslani F, Omran M. High-temperature mechanical properties of concrete. Int J Civil Eng. 2010;8:337–51.
25. Mustafaraj E, Yardim Y. Review of strengthening techniques and mechanical testing for unreinforced masonry. Matter: Int J Sci Technol. 2017;3:33–50. https://doi.org/10.20319/mijst.2017.32.3350.
26. ISO 834-1 (1999) Fire-resistance tests—Elements of building construction—Part 1: General requirements, International Organization for Standardization (ISO), Geneva, Switzerland
27. Daware A, Naser MZ. Fire performance of masonry under various testing methods. Constr Build Mater. 2021;289:123183. https://doi.org/10.1016/j.conbuildmat.2021.123183.
28. Beyazıt M, Yeğen Oğuz B. Statistics for engineers. Birsen Publishing; 2005.
29. Nacar S, Hınıs MA, Kankal M. Forecasting daily streamflow discharges using various neural network models and training algorithms. KSCE J Civ Eng. 2018;22(9):3676–85. https://doi.org/10.1007/s12205-017-1933-7.

Publisher's Note Springer Nature remains neutral with regard to jurisdictional claims in published maps and institutional affiliations.

Springer Nature or its licensor (e.g. a society or other partner) holds exclusive rights to this article under a publishing agreement with the author(s) or other rightsholder(s); author self-archiving of the accepted manuscript version of this article is solely governed by the terms of such publishing agreement and applicable law.